Pergamon

0967-0645(95)00041-0

Deep-Sea Research II, Vol. 42, No. 2–3, pp. 295–333, 1995
Elsevier Science Ltd
Printed in Great Britain

The 1991–1993 El Niño in the central Pacific

WILLIAM S. KESSLER* and MICHAEL J. McPHADEN*

(*Received for publication* 11 *April* 1995)

Abstract—The 1991–1993 El Niño event is described using data from the TOGA-TAO buoy network, concentrating on variability at 140°W where a full suite of temperature, current, and surface meteorological observations were made. The daily time series furnished by the buoy array brings out the conspicuous importance of remotely forced intraseasonal variability in the form of equatorial baroclinic Kelvin waves during the evolution of the 1991–1993 El Niño. Notable variations along 140°W included a major weakening of the Equatorial Undercurrent in late 1991 to early 1992, and a reduction in intensity of monthly period tropical instability waves during the latter part of 1991 compared to previous non-El Niño years. The North Equatorial Countercurrent showed no major signal due to this El Niño, in contrast to earlier warm events. Although anomalies of the South Equatorial Current spanning the equator were in an eastward sense during the height of the event, the result of these changes was that near-surface flow across 140°W between 5°S and 5°N was close to zero, so there was apparently no large eastward transport of surface water past 140°W into the eastern equatorial Pacific. The relative phasing of anomalies of thermocline depth, equatorial undercurrent speed and SST during the warm event of 1991–1992 was somewhat similar to that seen during the 1986–1987 El Niño, although the earlier event was followed by a strong cold (La Niña) event whereas the recent one was not. Uniquely among modern El Niño events, after the 1991–1992 episode appeared to end with a reappearance of the equatorial cold tongue in mid-1992, a second SST warming in the eastern Pacific occurred in early 1993.

The present data set is inadequate to fully diagnose the mechanisms of SST change at 140°W, but time series of insolation, air–sea temperature difference and humidity show that local air–sea heat flux variations (either radiative or turbulent) were probably not the primary cause of the SST changes during the El Niño. Similarly, although horizontal advective mechanisms were important contributors to SST signals at certain times, these alone did not account for the major warming and cooling events. Instead, the largest SST variations of the 1991–1992 El Niño can be ascribed to upwelling variations, and a simple parameterization for this process is presented. The major warming and cooling events in the central/eastern equatorial Pacific occurred nearly simultaneously over a wide longitudinal range, indicating that oceanic wave processes could not have been the sole source of the changes.

1. INTRODUCTION

The JGOFS (Joint Global Ocean Flux Study) EqPac cruises at 140°W took place against the background of the El Niño warm event of 1991–1992–1993 (Murray *et al.*, 1994). The purpose of this paper is to describe the development of the basin-wide circulation changes associated with this El Niño, with emphasis on conditions along 140°W, in order to place the physical/chemical/biological observations made during the JGOFS cruises in the context of their physical environment. Physical/dynamical issues raised by the JGOFS

*Pacific Marine Environmental Laboratory/NOAA, 7600 Sand Point Way NE, Seattle, WA 98115, U.S.A.

observations include the role of advection by the equatorial current system, large changes in the vertical structure associated with the passage of equatorial waves, upwelling variations, and changes in the air–sea fluxes. Sampling of the 1991–1993 event was more complete than in any previous El Niño due to the expanded TOGA-TAO (Tropical Atmosphere–Ocean) buoy array (Hayes *et al.*, 1991a; McPhaden, 1993), which is the primary data source used in this work. The daily time series of ocean temperature, currents and surface winds provided by the buoy network allows close resolution of the multiple time-scale features of the event.

Uniquely among modern El Niño events, after an apparent return to cool conditions in the eastern Pacific in the second half of 1992, another briefer, weaker warm event occurred in boreal spring 1993. We will use the terms "1991–1992 event" to refer to the warm event that began in September 1991, peaked in March 1992, and returned to cold sea-surface temperature (SST) in the eastern Pacific by August 1992, and "1993 event" to refer to the briefer warming in boreal spring 1993. The return of El Niño was particularly surprising since the generally accepted paradigm for El Niño assumed that warm events are preceded by a year or more of stronger than normal trade winds, which build up a thick warm layer in the western equatorial Pacific (Wyrtki, 1975; Battisti, 1988; Schopf and Suarez and Schopf, 1989). In a companion study, we tested hypotheses concerning the initiation and evolution of El Niño using basin-scale data from the TAO array (Kessler and McPhaden, 1995). Most notably, we found that the 1993 event was preceded by neither stronger than normal tradewinds nor a deeper than normal thermocline in the western Pacific, suggesting that present theories of El Niño do not completely account for the full range of observed interannual variability. This study complements that of Kessler and McPhaden (1995) by focussing more on descriptive aspects of the 1991–1993 El Niño along 140°W for the time period encompassing the JGOFS cruises; and by examining details of the upper ocean heat balance near the equator during the JGOFS time frame.

The high temporal resolution of the moored buoy observations brings out the conspicuous importance of variability at frequencies higher than are often considered in studies of El Niño. Two of these relatively rapid time scales are associated with particular phenomena: the intraseasonal Kelvin waves and the tropical instability waves, and we briefly review these here.

Intraseasonal (30–100 day period) variability of the tropical atmosphere is a global-scale phenomenon known as the Madden–Julian Oscillation (MJO) (Madden and Julian, 1971, 1972). The MJO usually arises over the central Indian Ocean as an organized region of deep convection. As this convection intensifies, it moves east at speeds of 3 to 6 m s^{-1} (Weickmann *et al.*, 1985; Rui and Wang, 1990; Weickmann and Khalsa, 1990). Typically the westerly winds below and to the west of the convection can be intense, and Kessler *et al.* (1995) showed the close connection between westerlies associated with MJO convection and generation of downwelling equatorial oceanic Kelvin waves in the Pacific. As the MJO moves east, past the edge of the west Pacific warm pool (about 160°E–180°), the convection and surface wind signature of the phenomenon weaken, so intraseasonal variability in the eastern Pacific Ocean is usually remotely forced (Kessler *et al.*, 1995). However, during El Niño, when warm SST above 28°C is found across the basin, MJO convection can penetrate to 140°W or even further east, and we will show observations of the occurrence of this during early 1992.

Tropical instability waves (TIW) are 20 to 30 day period oscillations first seen in satellite observations as an undulating SST front just north of the equator in the eastern Pacific

(Legeckis, 1977). Their energy source is probably associated with shear instability of the large-scale zonal currents, although precisely which shear zones are important remains unclear. The waves are typically absent during boreal spring, when the South Equatorial Current and North Equatorial Countercurrent are weak. Tropical instability waves produce large amplitude fluctuations of meridional current, with consequent strong advective temperature signals (Hansen and Paul, 1984; Pullen *et al.*, 1987; Halpern *et al.*, 1988; McPhaden, 1995). The three-dimensional TIW velocity field is only partly known, but appears to produce a net equatorial heat flux (Hansen and Paul, 1984).

2. DATA DESCRIPTION AND PROCESSING

2.1 *The TOGA-TAO buoy array*

The principal data set used in this paper is the TOGA Tropical Atmosphere–Ocean (TAO) buoy array, which consists of more then 60 deep ocean moorings arranged in pickets nominally 15° longitude apart across the equatorial Pacific (Fig. 1). Most of these buoys are ATLAS thermistor chain moorings (Hayes *et al.*, 1991a) that measure temperature at the surface and 10 subsurface depths down to 500 m, as well as surface winds, relative humidity and air temperature. Air and water temperatures and relative humidities are sampled 6 times per hour, and daily averages of these are transmitted in real time each day to shore by satellite via Service Argos. Vector winds 3.8 m above the surface are sampled at 2 Hz for 6 min each hour and similarly averaged to daily means and transmitted via Service Argos. Zonal and meridional currents, surface winds, air temperatures, relative humidity, shortwave radiation, SST and subsurface temperatures are measured by PROTEUS moorings at 110°W, 140°W, 165°E and 156°E on the equator. These moorings, the first of which was deployed at 0°, 140°W in 1990, are equipped with downward-looking Acoustic Doppler Current Profilers (ADCP) that telemeter velocity profiles in the upper 250 m (McPhaden *et al.*, 1990). Before 1990–1991, buoys at these locations were instrumented with mechanical current meters at six to eight depths between the surface and 300 m (McPhaden and McCarty, 1992). Data gaps of up to 10 days were filled at each

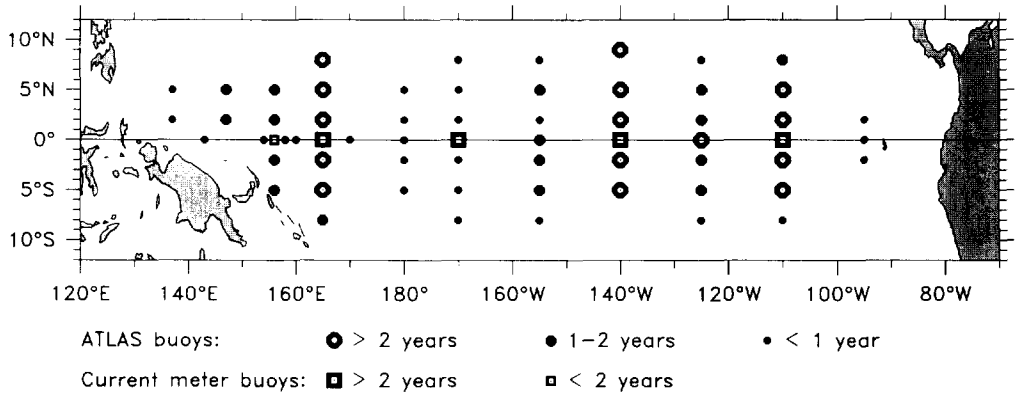

Fig. 1. Map of the TAO buoy network as of September 1993. The symbols indicate the length of time a buoy has been in the water at each location.

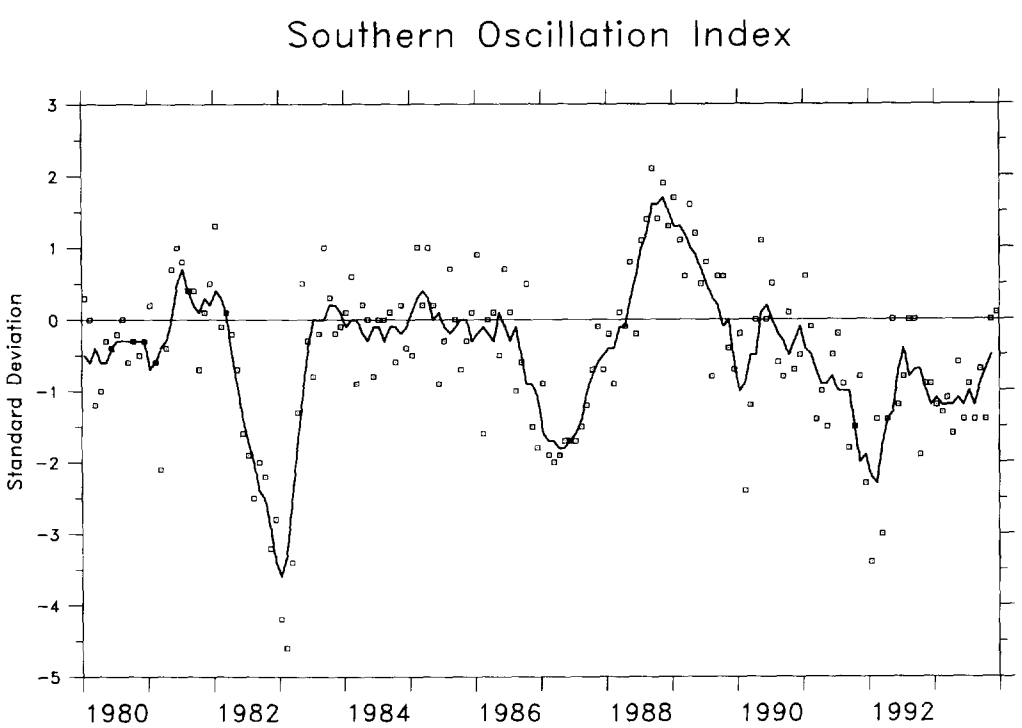

Fig. 2. Southern Oscillation Index (SOI). Monthly values (squares) and 5-month running mean (line). The SOI is based on the surface atmospheric pressure difference between Tahiti and Darwin, Australia. Negative values of the SOI indicate negative anomalies of surface pressure in the eastern Pacific, which are associated with El Niño.

location using an objectively estimated triangle filter having a half-power point at about 20 days (Chelton and Davis, 1982; Appendix). Time-longitude sections of zonal wind, SST and 20°C depth (Figs 3–5, respectively) were constructed by zonal linear interpolation. In a few cases where the equatorial mooring was not available, we used an average of the 2°S and 2°N time series to fill the sections.

For examination of the surface heat balance (Section 4), we have computed sensible, latent and longwave fluxes using daily averaged mooring data in the bulk formulae

$$Q_s = C_p^a \rho_a C_H U(T_0 - T_a) \tag{1a}$$

$$Q_L = L\rho_a C_E U(q_0 - q_a) \tag{1b}$$

$$Q_{LW} = [\varepsilon\sigma T_0^4(0.39 - 0.05e_a^{1/2}) + 4\varepsilon\sigma T_0^3(T_0 - T_a)](1 - 0.62C^2) \tag{1c}$$

where T_0 is SST, T_a is air temperature, U is wind speed, ρ_a is air density, q_a is the specific humidity at temperature T_a, q_0 is the saturation humidity for SST, e_a is the vapor pressure at temperature T_a, and C is the cloud fraction. C_E and C_H are turbulent exchange coefficients for latent and sensible heat, respectively, which we have estimated using Liu *et al.*'s (1979) formula, modified, based on recent TOGA-TAO measurements (C. Fairall, personal communication, 1994). L is the latent heat of vaporization, ε is the emissivity of

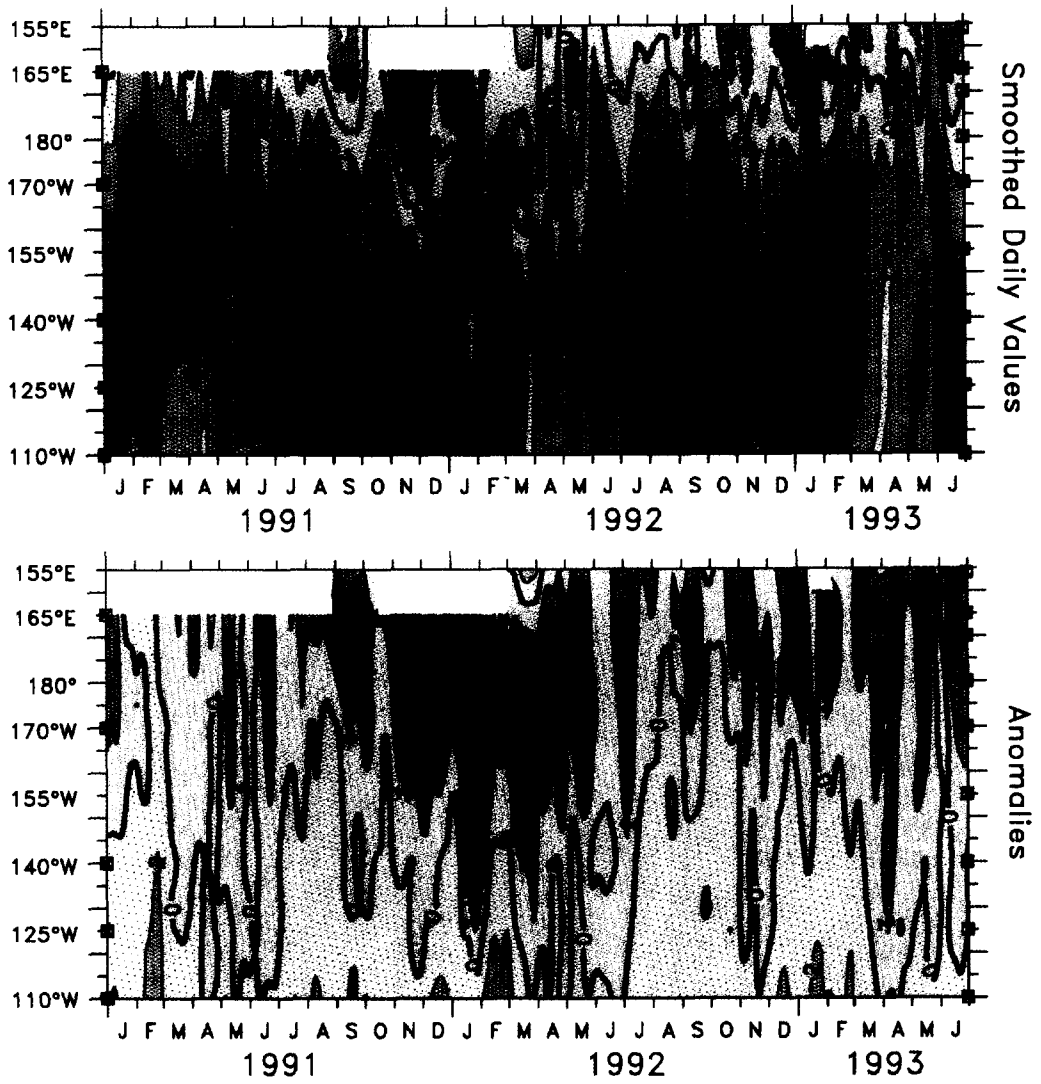

Fig. 3. Zonal wind (m s $^{-1}$) along the equator during 1991 through June 1993 from buoy data smoothed with a 17-day triangle filter. Top: observed values; bottom: anomalies from the COADS climatological annual cycle. Contours are every 3 m s $^{-1}$. Yellow to red shading indicates positive (westerly) zonal wind, blue indicates easterlies. Small squares along the left and right edges of the plots show the positions of the buoys used to make the gridded fields at the beginning and end of the study period.

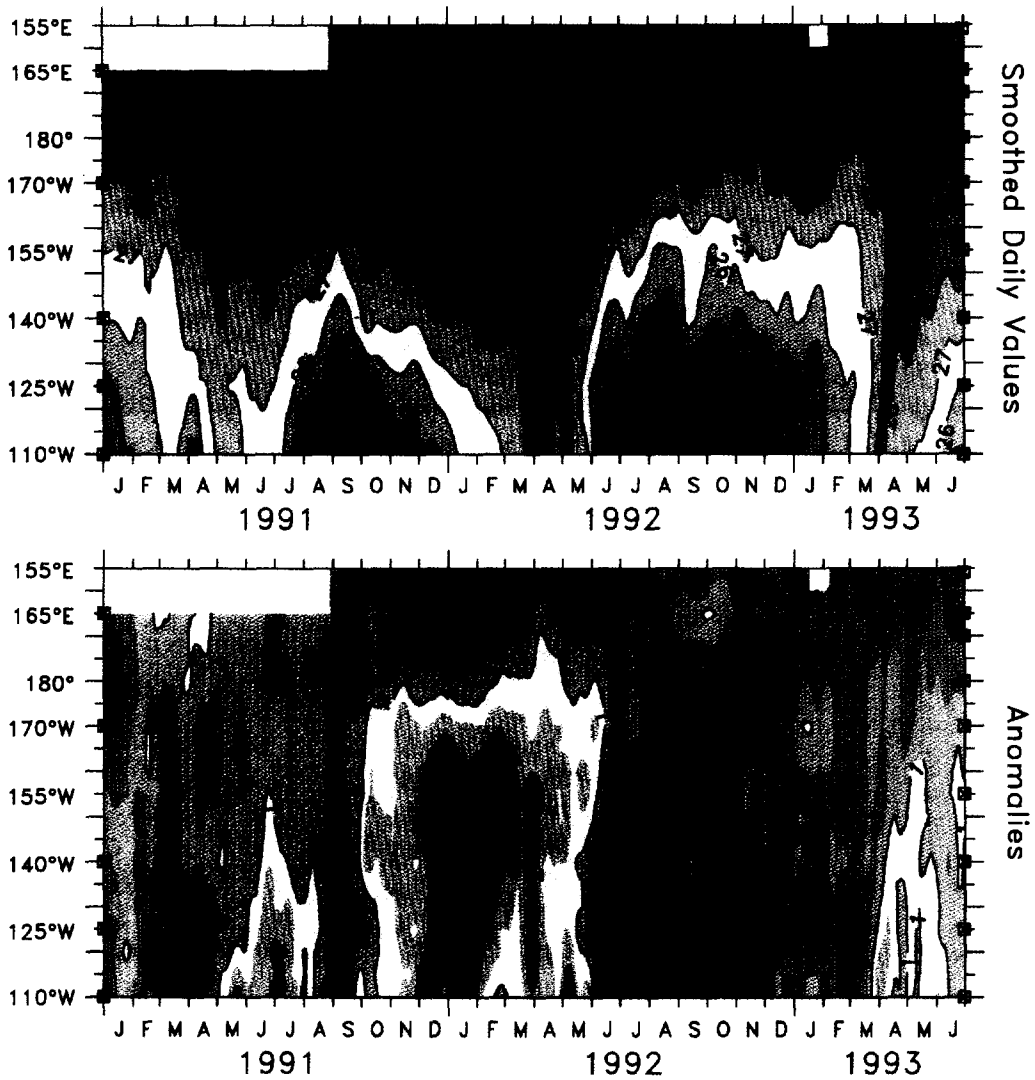

Fig. 4. As Fig. 3 except for SST (°C). Contours are every degree centigrade. Red shading indicates warmer SST, with a shading level every 1°C and a supplemental shading level to indicate 29.5°C. For the anomalies, shading levels are every 0.5°C.

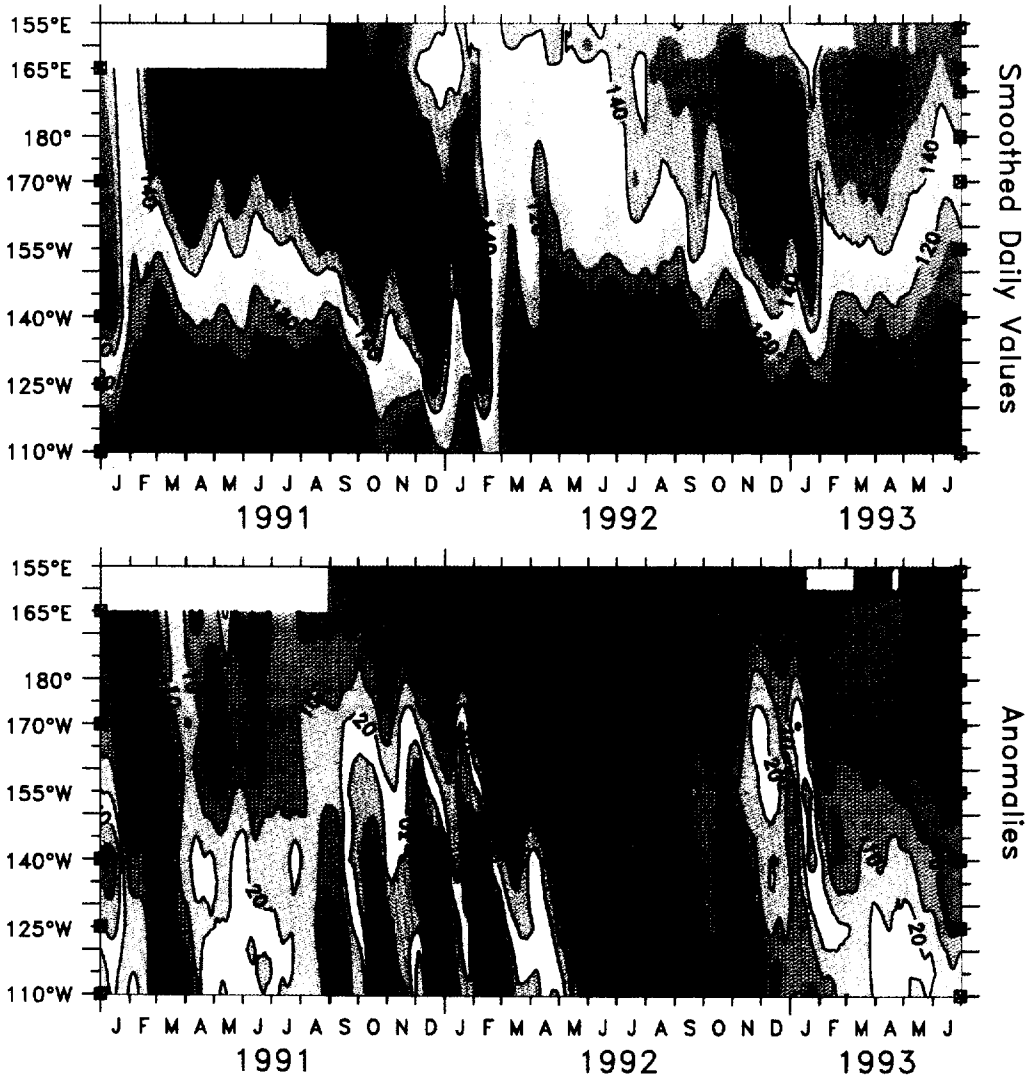

Fig. 5. As Fig. 3 except for 20°C depth (m). The contour interval is 20 m. Top: smoothed daily values. Bottom: anomalies from the annual cycle derived from XBT data. Red indicates deep thermocline, blue, shallow.

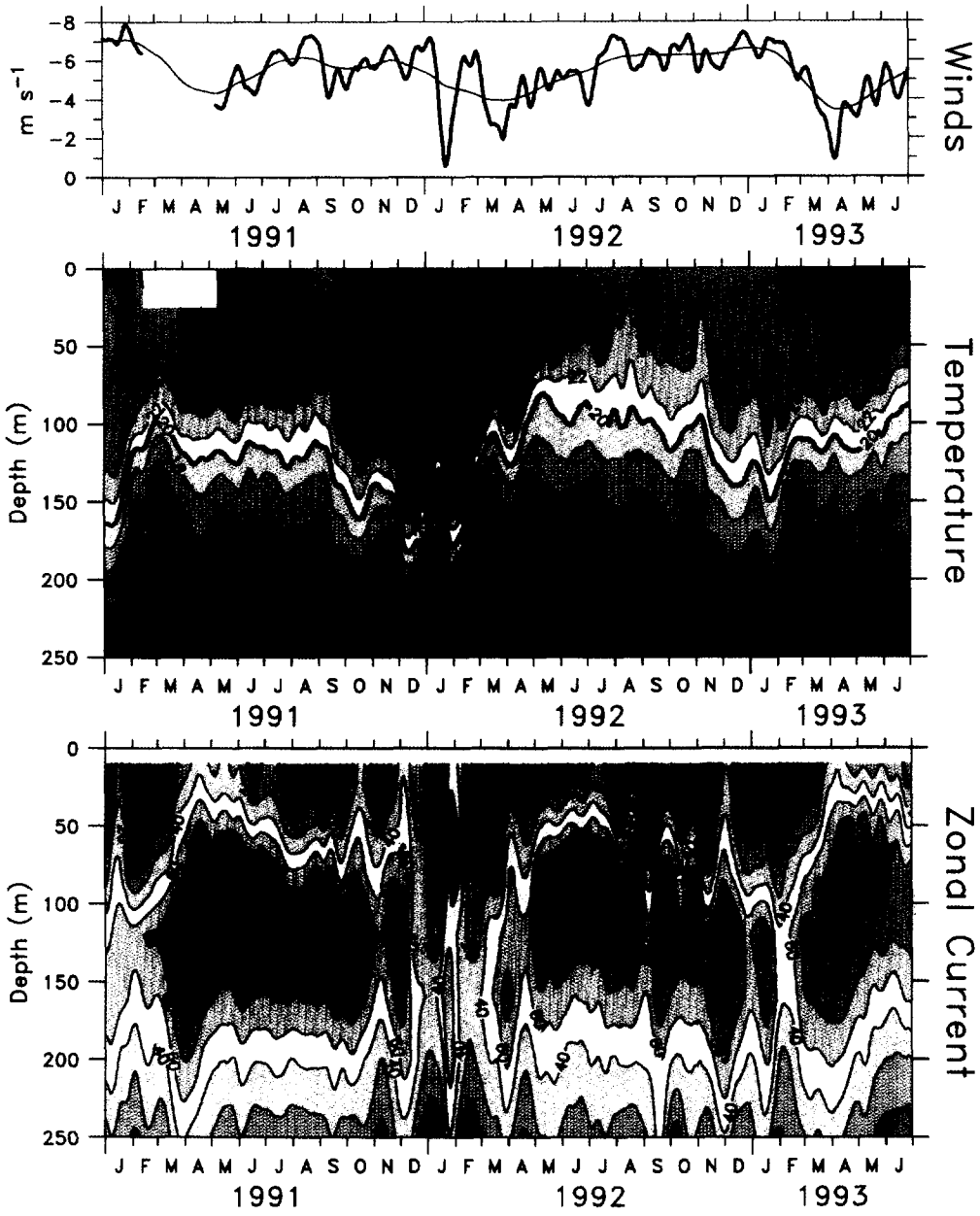

Fig. 7. Buoy winds, temperature and zonal current at 0°, 140°W during 1991 through June 1993, smoothed with a 17-day triangle filter. Top: zonal wind (m s^{-1}); middle: temperature between the surface and 250 m, with red indicating warmer temperatures; bottom: current (cm s^{-1}) between 10 m and 250 m, with red indicating positive (eastward) flow.

seawater, σ is the Stefan–Boltzmann constant, and C_p^a is the specific heat of air at constant pressure.

To obtain cloud fraction in the formula for Q_{LW}, we inverted Reed's (1983) expression for shortwave radiation using directly measured estimates of Q_{SW} from the Eppley precision pyranometer mounted at 3.5 m above mean sea level on the surface toroid at 0°, 140°W

$$C = 1.61\,[1 - (Q_{SW}/Q_{CS}) + 0.0019\eta] \tag{2}$$

where Q_{CS} is the clear sky radiation, Q_{SW} is measured insolation, and η is noon solar altitude. On occasion, this formula gave cloud fraction greater than unity for very low values of insolation, indicating that a more complete bulk parameterization of incoming shortwave radiation should include other cloud properties such as cloud optical thickness and/or cloud height. For the purposes of this study, we imposed an upper limit of $C = 1$ (fully cloud-covered sky) as computed from equation (2), although not imposing this limit has little discernable impact on the low-pass filtered time series of C and Q_{LW} discussed below. For short wave flux across the air–sea interface, we used directly measured values (available as 6-min averages every 20 min) reduced by 6% for oceanic albedo and averaged to daily mean. To confirm and extend time series of cloudiness values inferred from equation (2), we use outgoing longwave radiation (OLR), which is an indication of the occurrence of tropical deep convection obtained as satellite infrared radiance measurements (Weickmann *et al.*, 1985; Waliser *et al.*, 1993). Low values of OLR are assumed to be associated with tall cumulus towers and intense tropical convection. The OLR data discussed here are averaged into a 2.5° × 2.5° × 5 days latitude–longitude–time grid.

For typical instrumental errors in wind speed, air temperature, SST and relative humidity (Freitag *et al.*, 1994) the uncertainty in the determination of Q_L will be about 10 W m^{-2} (Zhang and McPhaden, 1995). Sensible heat flux itself is about an order of magnitude smaller than latent heat flux, and uncertainties in sensible heat flux at most will be only about 1 to 2 W m^{-2} due to instrumental errors. These error estimates for turbulent heat exchange do not include errors due to use of the bulk formulae (1) and (2); nor do they include possible sources of error arising from deployment at sea (e.g. buoy motion, radiational heating of the air temperature sensor, etc.). Such errors could be comparable to instrumental errors, but we have no way of evaluating them with confidence.

For shortwave radiation, Freitag *et al.* (1994) estimate a relative instrumental accuracy of 2%, equivalent to a 5 W m^{-2} error for typical solar irradiances of 250 W m^{-2}. For longwave radiation, estimates can vary by as much as 20 to 30 W m^{-2} depending on the form of the bulk formula used (Feng *et al.*, 1984); however this uncertainty would appear in our analysis mainly as a bias error with a lesser effect on temporal variability, which is the focus of our study.

We used the atlas of Oberhuber (1988) as a baseline to evaluate the representativeness of our latent, sensible and longwave surface-heat fluxes. Conversely, we used Reed's (1983) formula with the COADS (Woodruff *et al.*, 1987) cloud fraction to estimate a shortwave radiation climatology at 0°, 140°W. We found systematic biases of about 35 W m^{-2} in the measured shortwave vs the Oberhuber (1988) shortwave flux at 0°, 140°W over the entire period studied here. We ascribe this difference to the arbitrary reduction of surface shortwave radiation by 10% in Oberhuber's analysis, not to real interannual variability. The Reed/COADS computation gave a much more reasonable comparison to

the direct measurement in mid-1992 when SST and cloudiness returned to near-normal in the eastern Pacific cold tongue.

2.2 *TOGA XBT data*

Since the mid-1980s XBTs have been regularly deployed from volunteer merchant ships on a track between San Francisco and Tahiti, crossing the equator at 142°W, conveniently near the 140°W buoy line. During 1991–1992 a total of 913 XBT profiles (nominally to 450 m) were made on this line between 15°S and 15°N, for an average sample rate of 1.3 profiles per degree latitude per month. Previous studies using XBT data (e.g. Kessler *et al.*, 1985; Kessler and Taft, 1987; Picaut and Tournier, 1991; Taft and Kessler, 1991) have shown that this sample rate is adequate to construct meridional sections of the tropical Pacific zonal geostrophic currents, resolving variability with periods of longer than 2 to 3 months. These data are a useful supplement to the buoy time series, in particular for studying variations of the North Equatorial Countercurrent (NECC) at 4–10°N. This geostrophic current is not well resolved by the coarse meridional spacing of the TAO buoys, but can be an important component of the zonal redistribution of water during El Niño (Wyrtki, 1974; Meyers and Donguy, 1984; White *et al.*, 1985; Kessler and Taft, 1987).

To produce the time series of zonal geostrophic currents in Fig. 6, we first grouped profiles on the San Francisco–Tahiti ship track, defined as a swath 10° longitude wide, centered on the mean track position. Once the profiles were grouped within the track region, their longitude was ignored and the collection was considered simply as a meridional section approximately along 140°W (see Fig. 2 of Kessler and Taft, 1987). Having selected the profiles within the track region, density was found using a mean TS relation constructed from the Levitus (1982) climatology. Dynamic height was integrated for each profile separately (for all profiles extending to at least 300 m, and with at least 10 temperature samples), then gridded onto a 1° latitude by 1 month grid using a two-dimensional Gaussian-weighted moving average with mapping scales of 30 days and 1° latitude. The zonal geostrophic speeds shown in Fig. 6 were calculated by centered differencing the dynamic heights in the region poleward of 2° latitude.

2.3 *Other data sets*

Climatologies from several sources were used to define anomalies of observed quantities. For surface zonal wind speeds, anomalies were found from the COADS average annual cycle for the period 1946–1989. COADS is a monthly compilation (extending back into the 1800s) of surface meteorological observations from ships, binned on a global 2° by 2° grid (Woodruff *et al.*, 1987). SST anomalies were defined relative to the average annual cycle based on the most recent 10 years of the Reynolds and Smith (1994) blended satellite product. This is a weekly-average global product on a 1° latitude/longitude grid constructed from AVHRR data obtained from polar-orbiting satellites, adjusted to *in situ* data from ships and buoys, and gridded using an optimal interpolation procedure. Anomalies of 20°C isotherm depth were estimated from a climatology based on XBT/MBT data compiled by Kessler (1990), consisting of 21,811 profiles between 5°N and 5°S taken during 1970 to 1987. The terms "normal" and "climatology" in the text refer to the COADS, Reynolds and Smith (1994) and Kessler (1990) annual cycles, for winds, SST and 20°C depth, respectively. We have used these external climatologies rather than constructing

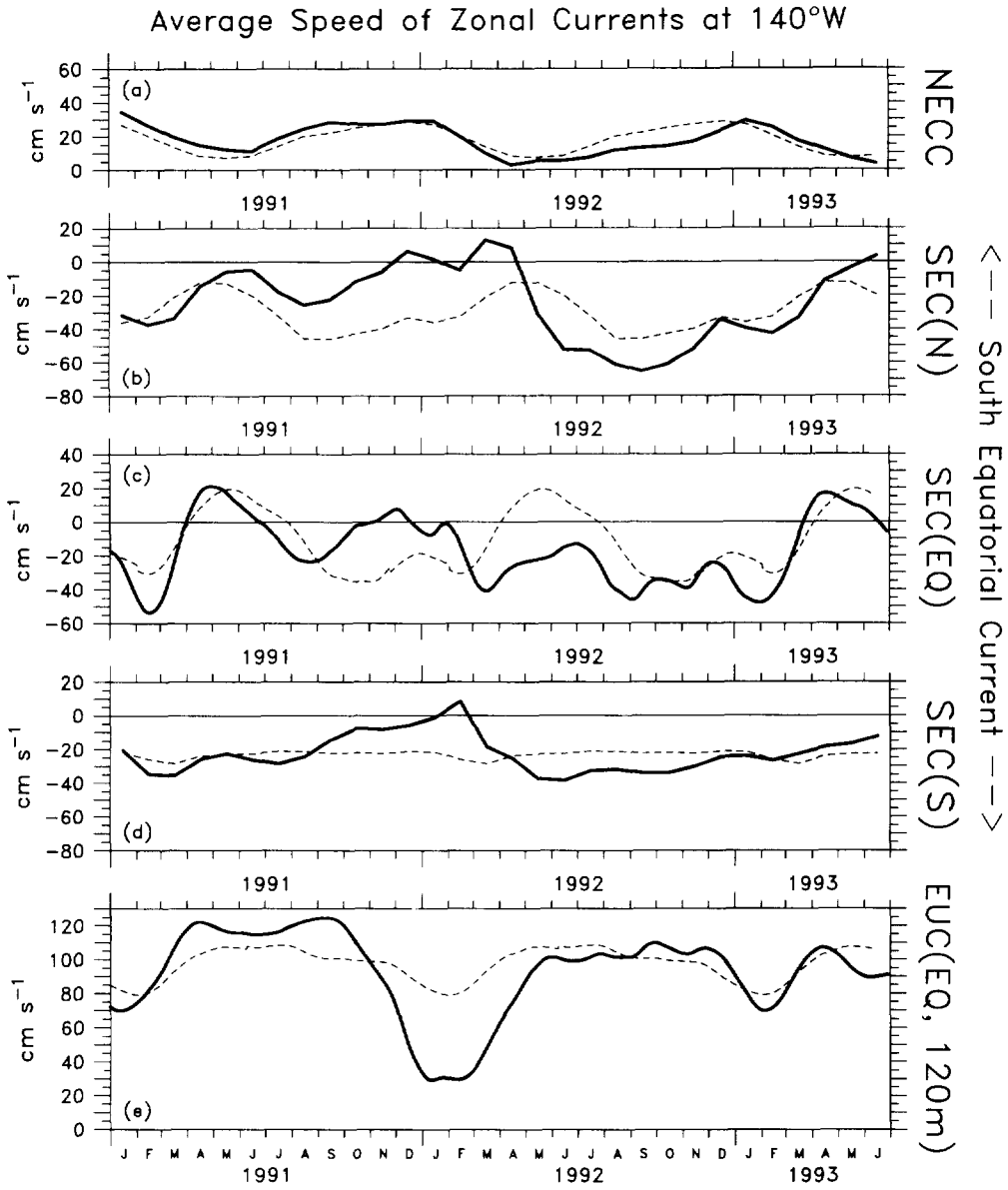

Fig. 6. Speeds of zonal currents at 140°W in five latitude bands. The dashed line is the average annual cycle in each case. For the off-equatorial currents [panels (a), (b), (d)] the speeds are geostrophic, relative to 300 m, and averaged in the latitude bands indicated. Panels (c) and (e) show directly measured speeds at the equatorial current meter buoy. The vertical scale is the same for each panel, and eastward flow is always shown positive (up). No attempt was made to calculate geostrophic speeds within 2° of the equator. (a) Surface zonal velocity averaged between 5°N and 11°N, approximating the North Equatorial Countercurrent (NECC); (b) as panel (a) but between 2°N and 4°N, approximating the South Equatorial Current (SEC) north of the equator; (c) measured zonal speed at the equator at 10 m depth, representing the SEC on the equator; (d) as panel (a) but between 2°S and 7°S, approximating the SEC south of the equator; (e) as panel (c) but at 120 m depth, representing the core of the Equatorial Undercurrent (EUC).

them from the buoy data itself, since most buoy records are relatively short (less than 10 years duration) and cover different time periods at different locations. The bottom panels of Figs 3, 4 and 5 show time–longitude sections of anomalies from these climatologies of zonal winds, SST and 20°C depth along the equator.

The Reynolds and Smith (1994) blended satellite SST product also was used to supplement the TAO buoy data when finer spatial resolution was needed. Comparison with the TAO buoy time series shows that the satellite analysis agrees well with the buoys at their locations, but adds a considerable amount of information on the zonal variation of SST between the 15° longitude spacing of the buoy lines. This is particularly important when variability due to tropical instability waves, which have zonal wavelengths comparable to the zonal separation of the buoys, is present. This data set also gives somewhat finer meridional resolution of the SST field (1° latitude for the blended product vs 2° latitude for the buoys), which we take advantage of in calculating the meridional derivative of SST.

3. CHRONOLOGY OF THE EVENT

3.1 *Before September* 1991

During 1990, persistent westerly wind and warm SST anomalies in the western equatorial Pacific had led to speculation that an El Niño event would begin in late 1960 (Kerr, 1990, 1991). However, it was not until September 1991 that observations could be unambiguously interpreted as El Niño. Surface winds across most of the basin during mid-1991 were typically within 1 to 2 m s^{-1} of climatology: anomalies were westerly during March to June, then weakly easterly during July to August (Fig. 3). SST west of the dateline remained close to 1°C anomalously warm during all of 1991. SST east of about 150°W was roughly 1°C above climatological normal during May to July 1991, but cooled more than 2°C during July and August to a level below climatology by mid-September (Fig. 4); this cooling occurred simultaneously with maxima of easterly winds, westward zonal surface current and upwelling in the eastern Pacific (Fig. 7). In September, thermocline depths along the equator and equatorial undercurrent speeds were close to their climatological values. It is therefore difficult to find a clear signature in the observations as of late boreal summer 1991 that an El Niño was underway.

3.2 *Development of warm SST anomalies: September* 1991 *to April* 1992

In late August 1991, the first of several strong Madden–Julian intraseasonal events moved into the western Pacific, with enhanced convection and westerly winds west of the dateline. The intraseasonal westerlies had two maxima during September, each lasting about 10 days (these synoptic-scale signals have been called "westerly wind bursts"). The anomalies were large in the west (4–6 m s^{-1} at 165°E), moderate (about 2 m s^{-1}) west of about 160°W (Fig. 3), but zonal winds at 140°W still gave no sign of the oncoming event. The westerlies generated a downwelling equatorial Kelvin wave that propagated east from the dateline region at about 2.4 m s^{-1} (Kessler *et al.*, 1995), arriving at 110°W at the end of October (Fig. 5).

In September, before the first Kelvin wave arrived, equatorial SST warmed nearly simultaneously between 125°W and 155°E (Fig. 4). The zonal coherence of this signal is emphasized by the abrupt sign change of d(SST)/dt calculated from the Reynolds and

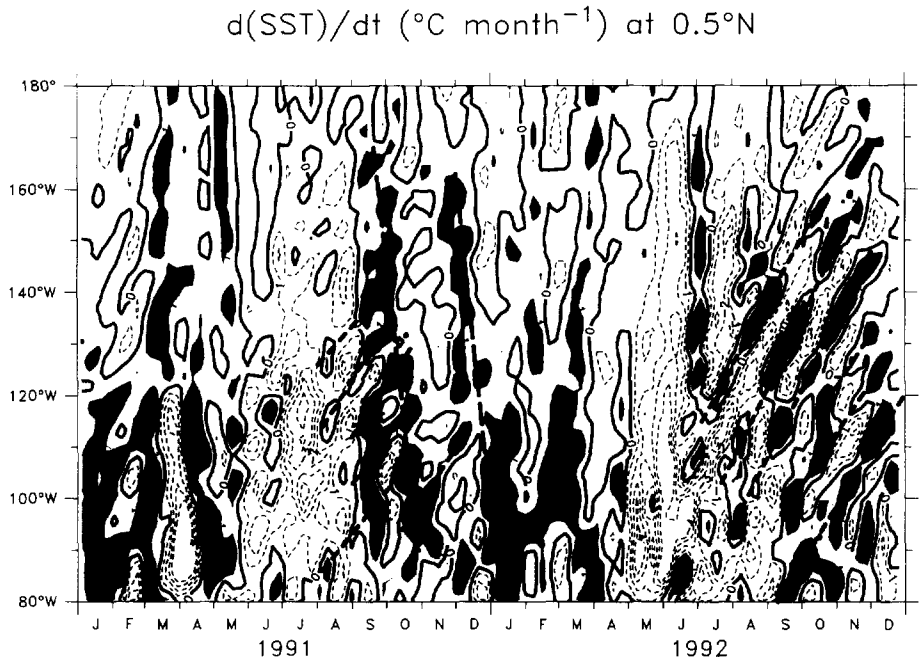

Fig. 8. Time rate of change of SST (°C month $^{-1}$) along 0.5°N, calculated from the Reynolds and Smith (1994) satellite-based product. The contour interval is 1°C month^{-1}, and shading indicates warming or cooling greater than 1°C month^{-1}. Dashed lines indicate warming signals due to identified waves: long dashes are Kelvin waves, while short dashes are tropical instability waves.

Smith (1994) satellite SST product (note the nearly vertical zero contour of d(SST)/dt in early September in Fig. 8). This warming occurred too early at 140°W to be due to the Kelvin wave (also the simultaneity across 8000 km argues against a wave process), but instead seemed to be associated with the weakening of easterly winds across the central Pacific in September (Fig. 3; see also Section 4). The Reynolds and Smith (1994) analysis establishes that, although eastern equatorial SST was being affected by a group of tropical instability waves at the time the SST rise began, the primary warming signal was independent of this wave field, as warming occurred across the eastern Pacific and thus during all phases of the waves (Fig. 8). However, the additional presence of the instability waves makes distinguishing among the various signals difficult, and at 140°W, their cycle was such as to contribute to the suddenness of the initial SST rise (Fig. 9) (see Section 4.2). The net warming east of 180° from mid-September to mid-October was between 1 and 2°C. In September the SOI turned below −1 and began a period of sustained large negative values (Fig. 2).

By mid-October 1991 the phase of the MJO had reversed and westerly wind anomalies were nearly gone from the equatorial Pacific, with easterlies observed everywhere east of

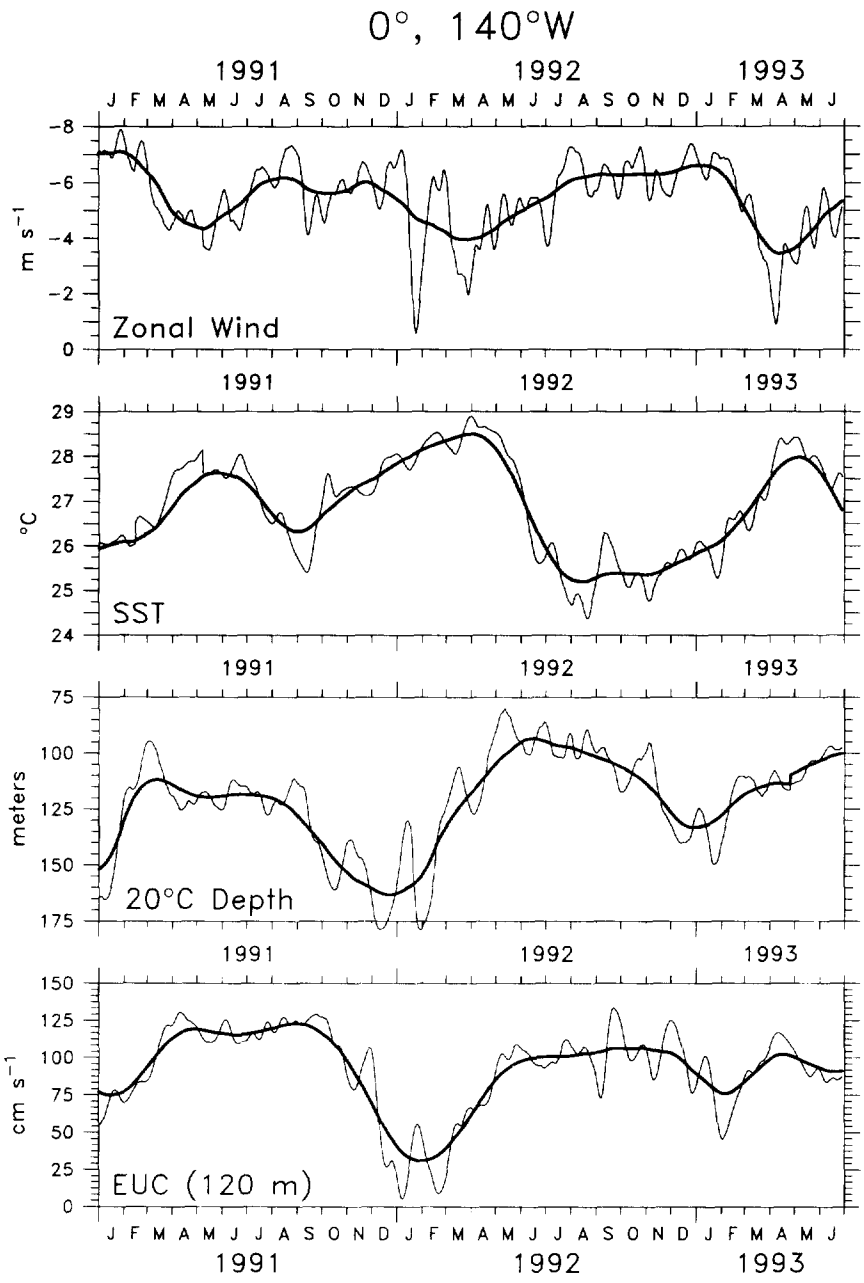

Fig. 9. Zonal wind, SST, 20°C depth and Equatorial Undercurrent speed at 0°, 140°W during 1991–June 1993. All have been filtered with a 17-day triangle (heavy line), and with a 121-day triangle (light line). Top: zonal wind (m s^{-1}); second: SST (°C); third: 20°C depth (meters); bottom: zonal current at 120 m (cm s^{-1}).

165°E (Fig. 3). Weak cooling of SST (about 0.5°C during the first two weeks of October) occurred in the central Pacific (Fig. 9). However, the arrival in the east of the Kelvin wave that had been generated near the dateline in September produced sharp downwelling of the thermocline during October: 20 m at 155°W, 40 m at 140°W, and more than 50 m at 110°W (Fig. 5). The wave was associated with a short-lived pulse of anomalous eastward current (about 40 cm s^{-1}, lasting for about two weeks) coherent from at least 100 m to the surface, observed at 140°W (Fig. 7) and 110°W.

In mid-November 1991, convection and westerly winds returned to the western Pacific as the second Madden–Julian intraseasonal event propagated into the region. The two-month separation between events is typical of the Madden–Julian cycle. The November westerlies were about twice as strong as those of September, and extended much farther east. Westerly winds were observed to 155°W (Fig. 3), with strong westerly anomalies (more than 10 m s^{-1}, even in the smoothed time series) west of the dateline. However, zonal winds during December continued to be seasonally normal at 140°W, and anomalously easterly at 110°W (Fig. 3). The November westerlies generated a second downwelling Kelvin wave which again propagated at close to 2.4 m s^{-1}, peaking at 110°W just at the end of the year (Fig. 5). The amplitude of the second wave was similar to the first, with 20°C isotherm vertical displacements of 30 m at 170°W, and 40–50 m east of 155°W. At the peak of this wave in late December, all isotherms from 27°C to 14°C at 140°W and 110°W were deeper than at any time since December 1982 (generally about 20 m deeper than at the peak of the 1986–1987 event), so that, by this measure, the 1991–1992 event could be categorized as a strong El Niño. The second wave again produced vertically coherent 40 cm s^{-1} pulses of eastward current at 140°W (Fig. 7) and 110°W in early and middle December, respectively. After having been fairly constant during November, SST between 155°W and 110°W increased about 1°C during December (Fig. 8); unlike the first warming in late September, this rise was caused by zonal advection (discussed in Section 4.2 below) associated with the eastward pulse of current at 140°W and 110°W.

The Kelvin waves served to carry the westerly wind driven downwelling signal into the eastern Pacific, where they resulted in lowering the thermocline and thus reducing the zonal pressure gradient which drives the undercurrent. Thermocline depth anomalies were larger towards the east (Fig. 5, bottom), and the zonal thermocline slope west of 140°W was near zero or reversed from mid-November 1991 until the end of March 1992. Although the individual downwelling Kelvin waves produced brief eastward current pulses as they passed 140°W (Fig. 7), the low-frequency change in the Equatorial Undercurrent (EUC) during the onset period was a weakening of eastward flow (Fig. 6; Fig. 7), as has been observed in previous events (Firing *et al.*, 1984; Halpern, 1987; McPhaden and Hayes, 1990). The reversed zonal pressure gradient also indicates that the meridional geostrophic inflow towards the equator was reduced or absent at this time.

The large anomalies of temperature and dynamic height during December were mostly confined between 5°S and 2°N (Fig. 10), so there was little effect on the NECC, which occurs north of 4°N. Previous studies (e.g. Wyrtki, 1979; Taft and Kessler, 1991) had noted that the central Pacific NECC increases in strength during the onset phase of El Niño. However, throughout the onset and peak of the 1991–1992 event, NECC core speed between 4°N and 10°N at 140°W was very close to its climatological value (Fig. 6). On the other hand, the raised dynamic heights spanning the equator resulted in strong eastward geostrophic surface flow anomalies (20 cm s^{-1} or more) in the region usually occupied by the westward South Equatorial Current (SEC) (Fig. 6). This was consistent with directly

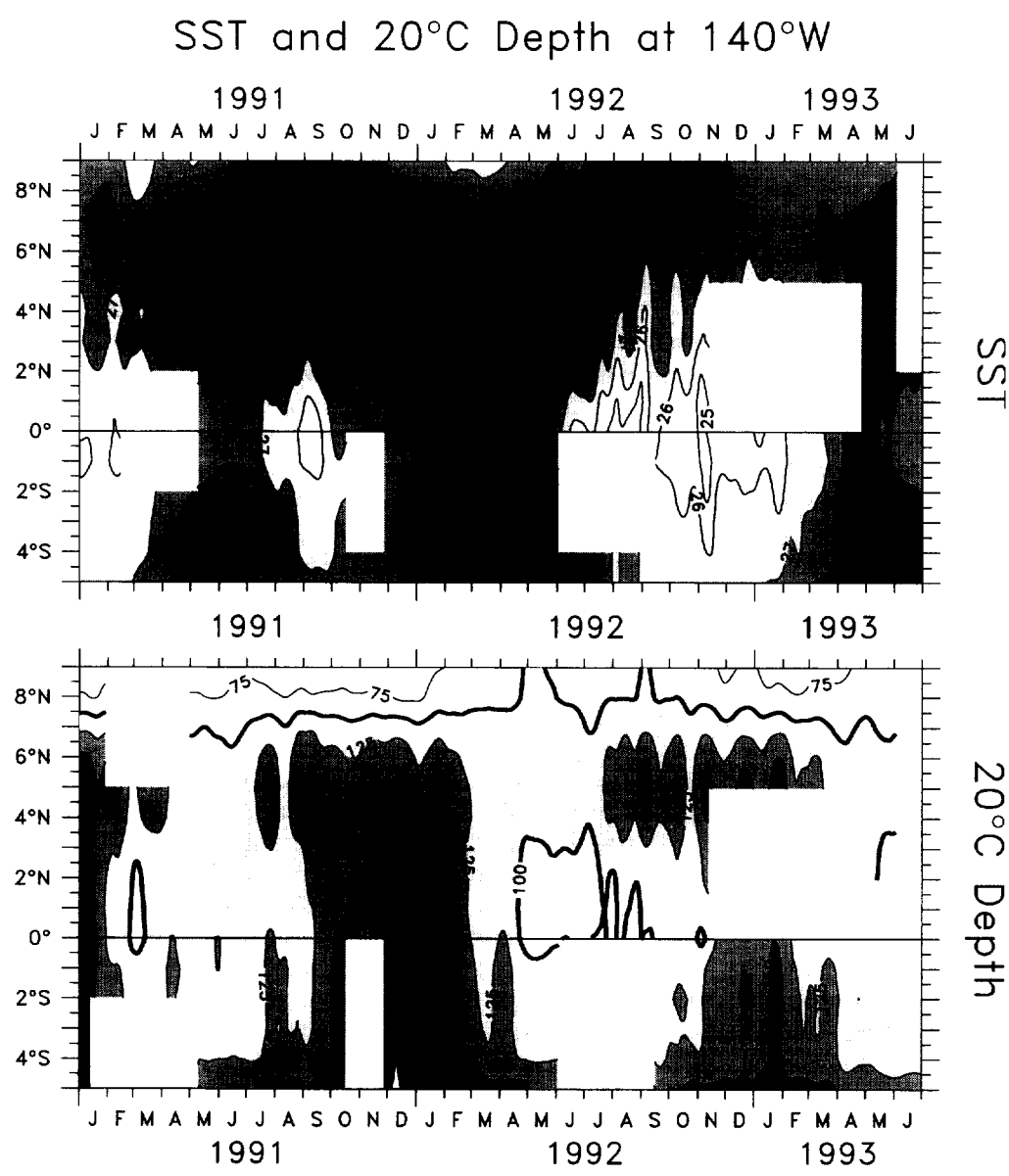

Fig. 10. Time–latitude sections of smoothed (17-day filtered) daily values of SST and 20°C depth at 140°W during 1991 through June 1993. Top: SST. The contour interval is 1°C and darker shading indicates warmer SST. Bottom: 20°C depth. The contour interval is 25 m and darker shading indicates deeper thermocline. Blank areas indicate missing data.

measured near-surface flow on the equator which indicated a similar weakening of the equatorial SEC at this time (Fig. 6). The overall result of these changes was that surface zonal flow across 140°W was near zero between 7°S and 4°N, and close to normal between 4 and 10°N, during the peak of El Niño from about November 1991 through February 1992

(Fig. 6). At the same time the EUC was also notably weak. Although it is difficult to accurately estimate total transport across 140°W, it is clear from these observations that there was no large transport of surface water from the west Pacific past 140°W into the eastern equatorial Pacific as part of the 1991–1992 event, as had been suggested by early ideas about the ENSO cycle (Wyrtki, 1975, 1979, 1984). Studies of the 1986–1987 El Niño similarly indicate that particle displacements from the west Pacific warm pool did not extend far into the east (McPhaden and Picaut, 1990; Picaut and Delcroix, 1995). Figure 7 (bottom) shows that at 140°W during the 1991–1992 peak there was some sloshing back and forth at intraseasonal frequencies, but the speed and duration of these signals suggests zonal particle motion on the order of 500 to 1000 km, not a basin-scale eastward advection.

In mid-December in the west Pacific the MJO westerlies weakened again (Fig. 3), the thermocline began to rise (Fig. 5) and SST cooled (Fig. 4). This upwelling signal propagated at the free Kelvin wave speed past 140°W in early January (Fig. 5). There the thermocline shoaled rapidly back to approximately the depth observed before the downwelling wave passage (Fig. 7). However, in early January 1992, strong westerly winds returned to the western half of the basin in association with a third Madden–Julian event. The anomalous winds and convection extended about 2000 km further east than did the November episode with westerly winds observed as far east as 140°W for several days in late January (Fig. 9), and westerly anomalies found everywhere west of 110°W (Fig. 3). Kessler *et al.* (1995) associated this eastward excursion of the MJO with the penetration of SST warmer than 28°C into the central Pacific. The central and east Pacific westerly anomalies lasted about three weeks. The January westerly event had a similar effect on the thermocline and zonal currents as the previous one in November: a Kelvin wave with strong downwelling and a brief pulse of eastward zonal flow, peaking at the end of January at 140°W and lasting about 3 to 4 weeks (Fig. 7). SST at 140°W increased about 0.5°C in response to eastward advection during the eastward current pulse (see Section 4.2 below). The event marked the deepest level of the central Pacific thermocline, and the subsequent weakening of the EUC in February (to 20 cm s^{-1} in the core) resulted in the largest anomaly of this current during 1991–1992 at 140°W (Fig. 7).

In mid-February 1992 the westerlies which had extended to 140°W in January abruptly disappeared, replaced by easterlies everywhere between 110°W and 155°E (Fig. 3); winds east of 125°W were more than 2 m s^{-1} anomalously easterly during February. The ocean response to these easterly winds included strong local upwelling of the thermocline as well as excitation of an upwelling Kelvin wave which propagated to 110°W in early March. By this time the east Pacific thermocline was at near-normal levels, but in the west 20°C was 20–30 m anomalously shallow (Fig. 5), continuing the trend which had begun with the December easterlies.

A fourth, weaker Madden–Julian event occurred in mid to late March 1992, with westerly winds observed at 170°W and westerly anomalies greater than 2 m s^{-1} between about 170°E to 125°, a shorter zonal extent than the previous occurrences (Fig. 3). This event again produced a downwelling Kelvin wave and eastward current pulse; these were smaller than the earlier signals at 140°W (Fig. 7), and almost absent at 110°W. Because there was little zonal SST gradient at this time (Fig. 4), the eastward current associated with the wave had no effect on the surface temperature, unlike the previous two Kelvin pulses. Early April marked the peak SST in the eastern Pacific, roughly two months after the peak thermocline depth and zonal current anomalies (Fig. 9). At the time of maximum warm SST anomaly at 140°W, the thermocline and undercurrent had returned nearly to

their seasonally normal values, although the surface current was anomalously westward (Fig. 6). A lag in which maximum SST followed deep thermocline anomalies by several months was also seen during the 1986–1987 warm event at 140°W (McPhaden and Hayes, 1990).

3.3 *End of the* 1991–1992 *warm event*

The westerly winds at the height of the event were stronger at or slightly south of the equator, with consequent large upwelling wind stress curl near 5°S and 5°N in the central Pacific during January to April 1992. This positive curl was most prominent between about 150 and 180°W, and at 5°N amounted to roughly 10 m month^{-1} Ekman upwelling during January to March 1992. The 20°C isotherm in fact shoaled more than 20 m at 5°N between 140°W and 170°W at this time (Fig. 10). Kessler and McPhaden (1995) showed that the upwelling signal propagated west as a long Rossby wave, taking 3 to 4 months to reach the western boundary and reflect as an upwelling equatorial Kelvin wave. They further showed that by mid-1992 this reflected Kelvin wave was contributing to the reversal of the deep thermocline which had characterized the central Pacific during the warm peak, leading to the termination of the 1991–1992 El Niño. This sequence of events, in which winds associated with one phase of El Niño create the conditions for its own destruction via the propagation of Rossby and Kelvin waves, is described by delayed oscillator theory (Battisti, 1988; Battisti and Hirst, 1989; Suarez and Schopf, 1989; Wakata and Sarachik, 1991).

The shoaling of the central Pacific thermocline near 5°N due to wind stress curl is a common feature of the aftermath of El Niños. In addition to the basin-wide effects due to wave propagation it tends to locally weaken the meridional pressure gradient associated with the NECC, and the usual annual NECC minimum can be intensified at this time (e.g. in 1973, 1983 and 1987) (Taft and Kessler, 1991). Consistent with these earlier events, in April to May 1992 the NECC was reduced to a small remnant with maximum speeds less than 10 cm s^{-1} along the central Pacific XBT tracks, less than half its usual speed and extent at this time of year (Fig. 6). This was due both to the anomalously shallow thermocline stretching across the equator and to the deep thermocline at 9°N (Fig. 10). The same equatorial thermocline rise that contributed to weakening of the NECC also tended to strengthen the South Equatorial Current (SEC). As has occurred during earlier El Niños, the SEC spanning the equator was particularly strong beginning in April 1992 (Fig. 6), as the usual "springtime reversal" did not occur (McPhaden, 1993).

During May to June 1992, equatorial SST cooled rapidly everywhere east of the dateline, and by July the cold tongue was well-established with SST up to 1°C colder than seasonal normal from 110°W to 160°W (Fig. 4). North and south of the equator, surface temperature remained up to one degree warmer than climatology, however (Fig. 10). The equatorial cooling was similar to the initial warming in that it occurred nearly simultaneously across more than 8000 km of zonal distance (Fig. 8). The cooling occurred at the same time as the large westward surface current anomalies in the SEC (Fig. 6). However, although the SST changes appear consistent with SEC anomalies through zonal advection, we will show in Section 4.2 below, that this process did not account for the abruptness or large amplitude of the cooling.

The westerly wind anomalies which had dominated the eastern equatorial Pacific for the previous six months abated by July–August 1992, although westerlies persisted west of the dateline (Fig. 3). The equatorial thermocline rose to near-normal levels in the east but remained about 30 to 40 m anomalously shallow west of 170°W (Fig. 5). The shallow west

Pacific thermocline following warm events has been previously observed and is consistent with the hypothesis that El Niño serves the function of episodic drainage of the west Pacific warm pool (Wyrtki, 1975; Cane, 1983), although, as we have noted, the drainage apparently did not occur eastward across 140°W. The EUC returned to typical strength in May at 140°W (its usual annual maximum) and continued to be strong through the rest of 1992 (Fig. 7), although the undercurrent at 110°W remained somewhat weaker than usual.

Tropical instability wave (TIW) activity has been noted to be weak during El Niño years (e.g. 1986, 1987 and 1991) and strong during the cool-phase post-El Niño years (1984, 1988 and 1992) (Fig. 11). Between August 1992 and February 1993, strong TIW activity was observed along 140°W, as evident, for example, in the temperature time-series at 5°N (Fig. 12). The 1992 waves produced a high-amplitude approximately 30-day period oscillation of the temperature profile which was out-of-phase across the upper thermocline (the phase jump was at about 100 m and 24–25°C). Preceding the TIW period, during all of 1991 and through July 1992 the entire thermocline between 18°C and 26°C had moved highly coherently, with virtually no change in the vertical distance between these isotherms (light gray area of Fig. 12). When the TIW activity began, the thermocline appeared to spread, increasing the separation between 18°C and 26°C from about 40 m to nearly 150 m in less than 10 days. SST at 5°N dropped about 1°C during the cold phase of the waves (Fig. 12). In February 1993 the TIW activity stopped abruptly, and the central thermocline at 5°N tightened and resumed a lower-frequency motion. Although the data are not sufficient to determine precisely the processes that caused the anomalies seen in Fig. 12, it appears that meridional advection of the upper ocean thermal field by a depth-coherent meridional velocity would produce such fluctuations measured at a fixed point; these temperature changes at the 5°N buoy do not necessarily imply large changes in the vertical thermal structure in a Lagrangian sense (McPhaden, 1995). Figure 10 shows that 20°C depth fluctuations associated with the 1992 series of TIW were most prominent at 5°N, but their SST signature was observed south at least to the equator; also the equatorial zonal current was affected with pulses of zonal flow oscillating at 20 to 30 day periods (Fig. 9, bottom). Figure 8 shows that the TIW SST signal extended from near the South American coast at about 85°W to about 160°W during late 1992.

3.4 *The return of warm conditions in early* 1993

Many of the quantities observed in late 1992 showed variability typical of the aftermath of a warm event. The cool SST anomalies in the equatorial east and central Pacific (Fig. 4), the shallow west Pacific thermocline (Fig. 7), and the return of the SOI to values close to zero (Fig. 2) all suggested that cool conditions would continue for at least a year, as has been the case for other modern El Niños. However, SST remained about 1°C anomalously warm near 165°E (Fig. 4), and in boreal fall–winter 1993 a series of Madden–Julian convective events continued to bring westerly winds to the warm SST region west of the dateline (Fig. 3). These westerlies produced downwelling Kelvin waves similar to, although weaker than, a year previously (Fig. 5). During the first five months of 1993, westerly winds were nearly continuous west of 180°, punctuated at intervals of 30 to 60 days by stronger westerly episodes (Fig. 3). In March and April 1993, SST at 140°W rose about 2°C to more than 1°C above the usual seasonal maximum (Fig. 9), and similar anomalies stretched from 180° to at least 95°W. At the peak of anomalously warm SSTs, the SOI stood at slightly less than −1 (Fig. 2) and westerly wind anomalies also were observed far

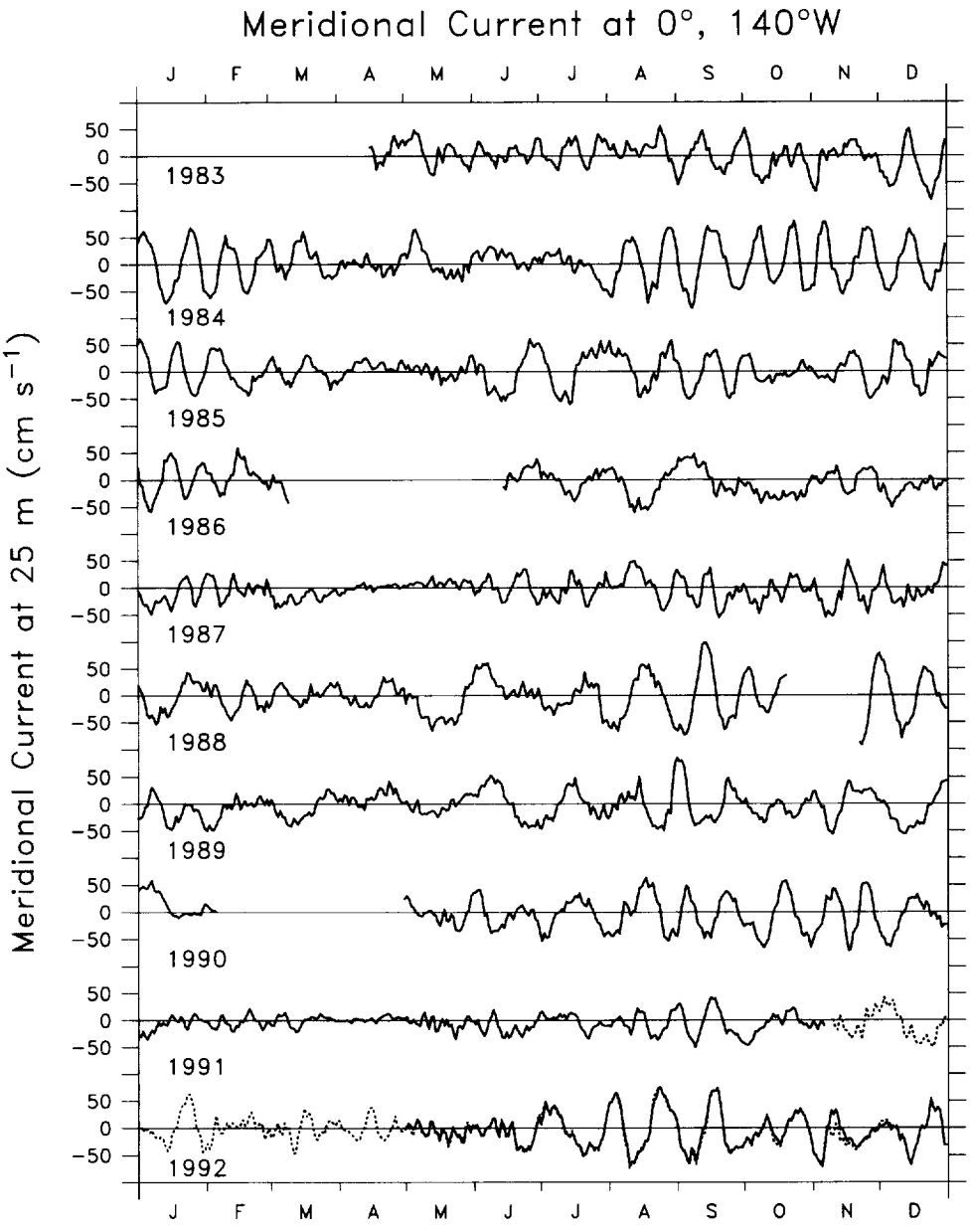

Fig. 11. Meridional current at 0°, 140°W, 25 m depth (cm s^{-1}), during 1983–1992. The six-month gap between November 1991 and April 1992 has been filled with the 10 m record (dotted line).

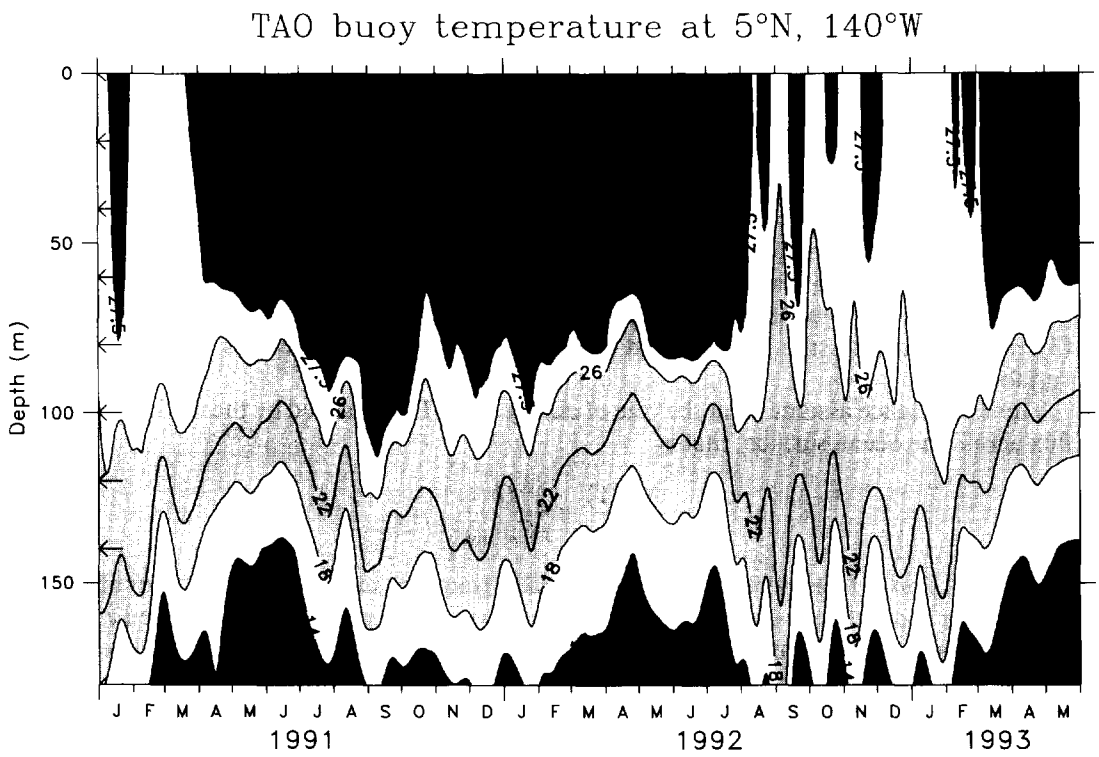

Fig. 12. Temperature at the 5°N, 140°W buoy during 1991 through to June 1993, smoothed with a 17-day triangle filter. Contours are every 4°C from 14°C to 26°C, then at 27.5°C and 28.5°C. Light gray shading indicates the thermocline between 18°C and 26°C, and dark gray shading indicates temperatures colder than 14°C and warmer than 27.5°C.

to the east, with near-zero zonal winds extending east to 0°, 125°E in early April (Fig. 3). By June this second warm event appeared to end as equatorial SST east of the dateline dropped to slightly below normal, and remained near normal for the rest of the year.

4. PROCESSES OF SST VARIABILITY

In this section we consider processes that may be of importance in affecting SST at 0°, 140°W during the 1991–1993 El Niño. The near-surface temperature balance is given by

$$\frac{\partial T}{\partial t} + u\frac{\partial T}{\partial x} + v\frac{\partial T}{\partial y} + w\frac{\partial T}{\partial z} = \frac{1}{\rho C_p}\frac{\partial Q}{\partial z} \tag{3}$$

where u, v, w are zonal, meridional and vertical velocity components, and x, y, z, t are longitude, latitude, depth and time, respectively. T is temperature, Q is the vertical heat flux, ρ is the density of seawater and C_p ($= 4000\,\mathrm{J\,kg^{-1}\,K^{-1}}$) is the heat capacity of seawater at constant pressure. Moored time series allow for explicit determination of the time rate of change of temperature, large-scale horizontal and vertical temperature gradients, and horizontal velocities. Also, solutions to equation (3) require a surface heat-flux boundary condition that can be estimated as $Q = Q_{SW} - Q_{LW} - Q_L - Q_S$ (the sign convention here is that positive Q indicates a warming influence on the ocean), where bulk formulae (Section

2.1) are used to estimate latent (Q_L), sensible (Q_S) and longwave (Q_{LW}) heat fluxes, and solar irradiance is estimated from directly measured shortwave (SW) radiation. Finally, although we cannot estimate vertical velocity explicitly, we devise a model that represents the effects of vertical advection in terms of explicitly measured changes in thermocline depth and local wind variations in order to test the idea that SST and thermocline depth are related in a simple fashion (McCreary, 1983; Zebiak and Cane, 1987; Battisti, 1988; Chang, 1994).

The 0°, 140°W buoy is one of the few locations where many of the quantities related to heat flux have been measured for a significant fraction of the 1991–1993 period. Even so, not all the records needed to test equation (3) spanned the complete time period of interest. Therefore, in this section we examine three different partial balances derived from equation (3), which optimizes the data needed to study subsets of the processes affecting SST variability.

The first balance assumes that the rate of change of SST is balanced by the net local heat flux across the ocean surface, that is

$$\frac{\mathrm{d(SST)}}{\mathrm{d}t} = \frac{Q}{\rho C_p h_{\mathrm{mix}}} \tag{4}$$

where equation (3) has been integrated vertically from the surface to the bottom of the mixed layer at depth $z = -h_{\mathrm{mix}}$. In this equation, advective terms have been ignored and it has been assumed that heat diffusion across the base of the mixed layer is negligible. There is a degree of arbitrariness in defining h_{mix}, which is inescapable in formulating equation (4). However, for our purpose we define h_{mix} as the depth at which the temperature is 0.5°C less than the SST, as was done by Hayes *et al.* (1991b) in a study of the mixed layer temperature balance at 0°, 110°W. Of course, this crude definition of h_{mix} does not represent a true mixed layer, but is simply a convenient approximation since we do not have concurrent salinity observations. During the 1991–1993 period, h_{mix} at 140°W defined in this fashion varied between about 110 m at the peak of deep thermocline anomalies in December 1991 to about 20 m in mid-1992, and averaged about 50 m. Despite the large fluctuations of h_{mix}, the conclusions we will draw from equation (4) are not particularly sensitive to the definition used, and similar results would have been obtained by using the mean value. Hayes *et al.* (1991b) also found a similar insensitivity to the form of h_{mix} in this kind of calculation.

The second balance is between horizontal advection and rate of SST change

$$\frac{\partial(\mathrm{SST})}{\partial t} = -u\frac{\partial(\mathrm{SST})}{\partial x} - v\frac{\partial(\mathrm{SST})}{\partial y} \tag{5}$$

where we assume surface currents are identical to those measured at the shallowest depth (10 m) from the moored ADCP. Test calculations using the Reynolds and Smith (1994) SST dataset, which has 1° longitude resolution, showed that the calculation of $\mathrm{d}T/\mathrm{d}x$ was relatively insensitive to the spacing of the zonal derivative, so our estimate of the zonal advection term from the moored time series should be reliable.

In contrast, neither the TAO buoys, spaced 2–3° of latitude apart, nor the satellite blended product (with values binned every 1° latitude, on the 0.5°) resolve the very sharp SST front usually found just north of the equator, which often exhibits a 3°C temperature change in less than 50 km (Pullen *et al.*, 1987). Thus, calculation of the meridional advection term $v\partial(\mathrm{SST})/\partial y$ at the equator can be very sensitive to how the derivative of

temperature is taken. For example, if centered differencing is done symmetrically about the equator, then $\partial(\mathrm{SST})/\partial y$ is nearly always close to zero (e.g. Fig. 10); however, if upstream differencing is performed, then $\partial(\mathrm{SST})/\partial y$ most of the time has the opposite sign as the meridional current. For upstream differencing, the term $v\partial(\mathrm{SST})/\partial y$ is therefore nearly always found to be strongly negative, regardless of the sign of the current, which reflects the generally equatorward eddy heat flux associated with the tropical instability waves (e.g. Hansen and Paul, 1984). In order to get the finest possible resolution of the meridional temperature gradient, we use 1° latitude upstream differencing based on the Reynolds and Smith (1994) satellite product in our estimation of the meridional advection term.

The third balance we examine is an attempt to parameterize upwelling-induced SST changes, which is the most difficult mechanism to evaluate quantitatively. A simple conceptual model of the vertical advection effect on SST might be that upwelling speed itself is proportional to the local wind stress through Ekman divergence, but the efficiency of upwelling to produce SST variations is controlled by the thermocline depth. If the upper layer is very deep, then even strong upwelling might not affect the SST; on the other hand if the thermocline is shallow, then even small wind signals could generate enough upwelling to be effective in cooling the surface. This is similar in spirit to parameterizations used in numerical models of the cold tongue region (e.g. Battisti, 1988). A simple functional form which expresses this kind of relationship is that SST is proportional to the ratio of zonal wind stress to thermocline depth, i.e.

$$\mathrm{SST} = A\frac{\tau^x}{\mathrm{Z23}} + T_0 \tag{6}$$

where A has units equivalent to depth divided by heat capacity, Z23 is the depth of the 23°C isotherm, and τ^x is the zonal wind stress divided by the density of seawater. Test calculations showed that similar results were obtained using any isotherm between about 15°C and 23°C, with some improvement in correlation for the shallower isotherms; we chose 23°C to represent a temperature level near the top of the thermocline but which rarely surfaces (Fig. 7). In equation (6), time series of SST, τ^x and Z23 are known from the buoy observations, and the constants A and T_0 can then be found by regression.

An important feature of the hypothesis (6) is the mixture of local wind forcing and the effects of remote winds which largely determine thermocline depth in the eastern equatorial Pacific. We do not expect this balance to hold on short timescales [note that there is no time derivative in equation (6)], but imagine that over periods of a month or longer mixing could have brought SST into equilibrium with prevailing conditions of wind stress and thermocline depth. Chang (1993), in an investigation of the seasonal cycle of the heat balance in the tropical Pacific mixed layer, found that SST could be approximately in phase with upwelling-driven vertical entrainment in the eastern equatorial Pacific where the thermocline is shallow and mixing is intense, consistent with the simple model presented here. On the other hand, he found that in most of the world ocean the balance was between net heating and the time rate of change of mixed layer temperature (Chang, 1993), so the balance (6) should not be thought of as generally applicable.

To review the chronology of SST change at 0°, 140°W, Fig. 9 shows the time history and Fig. 13 (bottom) the time derivative of SST measured at the mooring site. There were four principal warming events during the onset phase from 1991 to early 1992: in late September and early December 1991, and in late January and mid-March 1992. The first

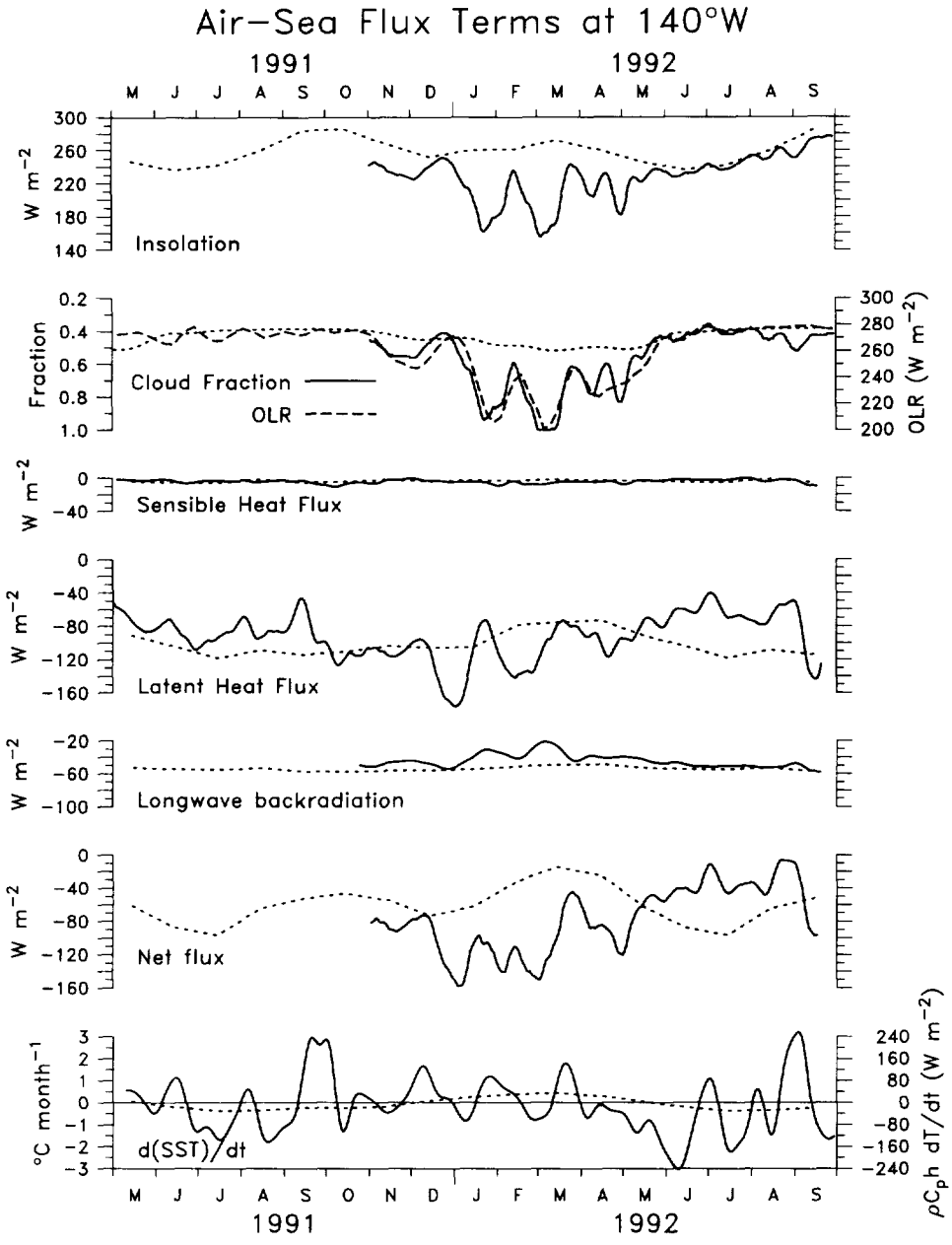

Fig. 13. Air–sea flux quantities at 0°, 140°W during 1991 through to June 1993. In each case the solid line gives the measured value at the buoy, and the short dashed line is the climatology (see text). Tendencies for ocean warming are shown as positive flux values and drawn up on the figure. All the flux quantities are plotted at the same scale. Top: insolation; second: cloud cover fraction (overlaid dashed line is satellite-derived outgoing longwave radiation, with its climatology in short dashes); third: sensible heat flux; fourth: latent heat flux; fifth: longwave back radiation; sixth: net flux (sum of insolation minus the sensible, latent and longwave fluxes); bottom: d(SST)/dt (°C month^{-1}). The right axis of the bottom plot shows the SST tendency scaled by $\rho C_p h$ to show units of heat flux (W m^{-2}) according to equation (4) (see text).

Table 1. *Surface layer heat-flux summary statistics at* 0°, 140°W. *Mean and RMS amplitude of the annual cycle and interannual variability*

Flux term	Mean	Annual cycle RMS	Interannual RMS
Shortwave radiation	260.6	13.6	29.6
Latent heat flux	−99.2	14.1	30.3
Sensible heat flux	−3.5	1.0	2.5
Longwave radiation	−53.7	2.6	9.0
Net air–sea flux	104.2	21.7	49.0
Zonal advection	−1.2	18.1	16.9
Meridional advection	68.7	8.3	37.9
Upwelling	~−170	~30	~60
$\rho C_p h_{\mathrm{mix}}$ d(SST)/dt	0	21.8	27.0

All quantities are in units of W m^{-2}, and mean values of all quantities are shown positive for a warming tendency in the ocean. The top five variables are the air–sea heat fluxes, calculated from the buoy observations using definitions (1). The mean and annual cycles of these are found from the climatologies discussed in Section 2.1. Interannual RMS of the air–sea fluxes is found from the difference between the climatologies and observations shown in Fig. 13. Note that these anomalies are for relatively short periods.

Heat fluxes due to zonal and meridional advection are found from the time series shown in Fig. 15, integrated over an upper layer of 50 m depth. The mean and annual cycles are for the period July 1986 through July 1993. Interannual anomalies are for the period January 1991 through July 1993.

Heat fluxes due to upwelling are estimated from the parameterization (6), with the additional assumptions in equations (7) and (8). Equation (8) was integrated over an upper layer of 50 m depth, with α calculated using $y_u = 3°$ latitude. These values are uncertain to at least a factor of two (see text).

The bottom line gives the amplitude of the total heat flux needed to produce the observed SST variability during the period July 1986 through July 1993, again assuming processes acting over a 50 m thick surface layer.

warming event was the largest, accounting for a nearly 2°C rise in about 20 days at 140°W, and Fig. 4 shows that the warming happened simultaneously between 110°W and 155°E. Peak SST was reached at the end of the series of warmings in March 1992, and very rapid cooling occurred during May–July 1992, again simultaneously across the entire zonal extent of the buoy region, so that by late July 1992 SST at 140°W was cooler than at any time since the 1988 extreme cold event. We now seek to identify potential mechanisms for these large fluctuations using equations (4), (5) and (6). Some of these results are summarized in Table 1, which gives the mean and the RMS magnitude of the average annual cycle and interannual variability of the surface layer heat balance terms. It should be kept in mind that the time periods during which the various terms could be studied were quite disparate, so that caution should be exercised when comparing relative interannual RMS magnitudes in Table 1.

4.1 *Air–sea heat fluxes*

Local air–sea flux quantities that enter into balance (4) at 140°W are shown in Fig. 13. Data in Table 1 show that the shortwave and latent heat fluxes were larger both in the mean and their annual and interannual variations than the other air–sea terms. Variations

of these fluxes at 140°W during the 1991–1992 event were associated with changes in wind speed, cloudiness and SST. The large insolation changes were due to increases in cloudiness as the Madden–Julian convection events penetrated to this region, and insolation is seen to vary at the MJO 60-day period (Fig. 13). Latent heat flux (LHF) fluctuations on timescales of less than about 90 days were largely due to changes in wind speed (weaker flux out of the ocean during low winds), but its low-frequency variability was primarily correlated with SST (higher flux at higher SST), as noted by Zhang and McPhaden (1995). The two largest LHF cooling events, in December and January of 1991 and 1992 and in February to March 1992 were due to strong easterly winds blowing over very warm SST (Figs 3 and 4). Sensible heat flux variations were insignificant compared to the other terms (Fig. 13; Table 1). The longwave flux out of the ocean was also relatively small (Fig. 13), and its variations were mainly due to increases in cloudiness reducing net longwave heat loss. Total flux variability was thus approximately the sum of the insolation and the latent heat flux (Fig. 13; Table 1). Unfortunately the radiometer at 140°W was first deployed in November 1991, so there are no direct *in situ* short wave flux measurements during the onset of warming earlier in 1991, and lacking this term it is not possible to calculate net flux from the observations for the entire 1991–1993 time period. However, we can infer that the insolation was probably near climatology during this time because the outgoing longwave radiation, which is a good indicator of cloudiness (the correlation between OLR and cloud fraction at 140°W was 0.95), was near normal until November 1991 (Fig. 13). These results suggest that net surface flux deviations during the initial SST warming in September to October 1991 were primarily due to anomalies of latent heat flux.

During the period when the total net flux can be calculated from the buoy observations, the SST tendency due to air–sea fluxes was anomalous cooling from November 1991 until April 1992, and anomalous warming from May to August 1992. The cooling tendency was associated both with the reduction in insolation due to increased cloudiness and the two large latent heat-flux events (Fig. 13); the net heat-flux anomaly amounted to about 80 to 120 W m^{-2}. According to equation (4), this anomalous flux would have produced about 1 to 1.5°C $month^{-1}$ cooling relative to climatology, if no other processes were at work. The total cooling would have been about 4°C between November 1991 and April 1992. However, SST in fact warmed about 0.5°C relative to climatology during this period, so the air–sea flux tendency was of the wrong sign to produce the observed SST changes.

In May 1992 the air–sea flux tendency changed sign, and during the next four months the net flux represented an anomalous warming tendency of about 40 to 60 W m^{-2} (Fig. 13). Since the mixed layer, h_{mix}, was quite shallow at this time (Fig. 7), the effect on SST as hindcast by equation (4) was relatively large, amounting to up to 1°C $month^{-1}$, and the time integrated SST change due to this warming tendency would have been as large as 4°C. However, during this period observed SST fell more than 3°C, so, as in the earlier period, the actual SST change was opposite to that expected from the air–sea flux tendency.

If the inference made above, that cloudiness and insolation were near-normal during mid-1991, is correct, then anomalies of air–sea flux were due largely to the latent heat flux at that time. LHF was observed to be smaller than climatology by about 20 to 50 W m^{-2} before October 1991, representing an anomalous heat gain for the ocean (Fig. 13). This anomalous warming tendency was due to the abrupt weakening of zonal winds in mid-September (Fig. 9, top) reducing evaporative cooling. Thus the LHF was of the right sign to have played a role in the initial SST warming in September 1991, when it peaked at about 50 W m^{-2} above climatology. However, according to equation (4), if latent heat flux

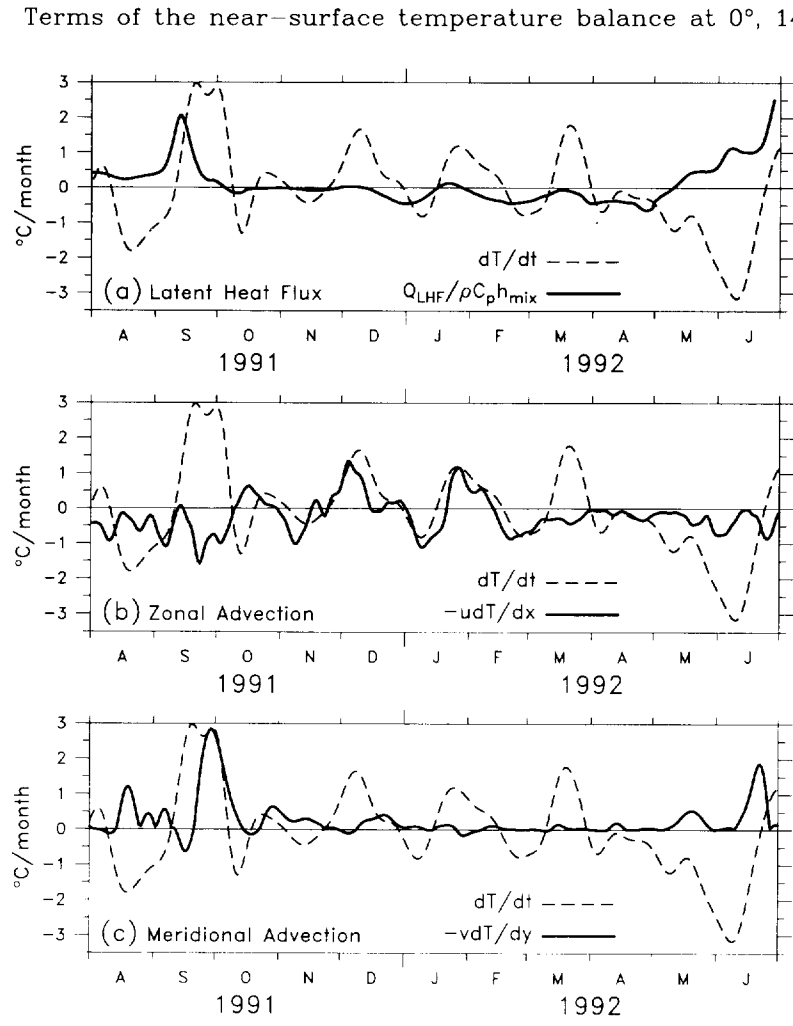

Fig. 14. Terms of the near-surface temperature balance (°C month^{-1}) at 0°, 140°W during the warm event of 1991–1992. In each case the dashed line is $\partial SST/\partial t$, while the solid line is an SST tendency term. (a) Anomalies of the latent heat flux term $Q_{LHF}/\rho C_p h_{mix}$; (b) the total zonal advective term $-u\partial SST/\partial x$; (c) the total meridional advective term $-v\partial SST/\partial y$. The advective terms are drawn with signs as in equation (5) (tendencies for ocean warming drawn up on the plot).

were the primary control on SST, the September LHF anomaly would have corresponded to about a 0.7°C upper layer temperature increase. This increase was only one-third that observed, suggesting that other oceanic processes must have been important. Figure 14(a) compares the time rate of change of SST with the LHF effect according to equation (4) ($Q_L/\rho C_p h_{mix}$). The LHF term was small except during mid-September 1991, when it appears to have contributed to the initial SST warming, and during May and June 1992, when it became large due to the very shallow mixed layer (as suggested by Fig. 7), but was of the opposite sign as the observed cooling. There was some degree of correlation between SST change and latent heat flux variations during January and March 1992, but it

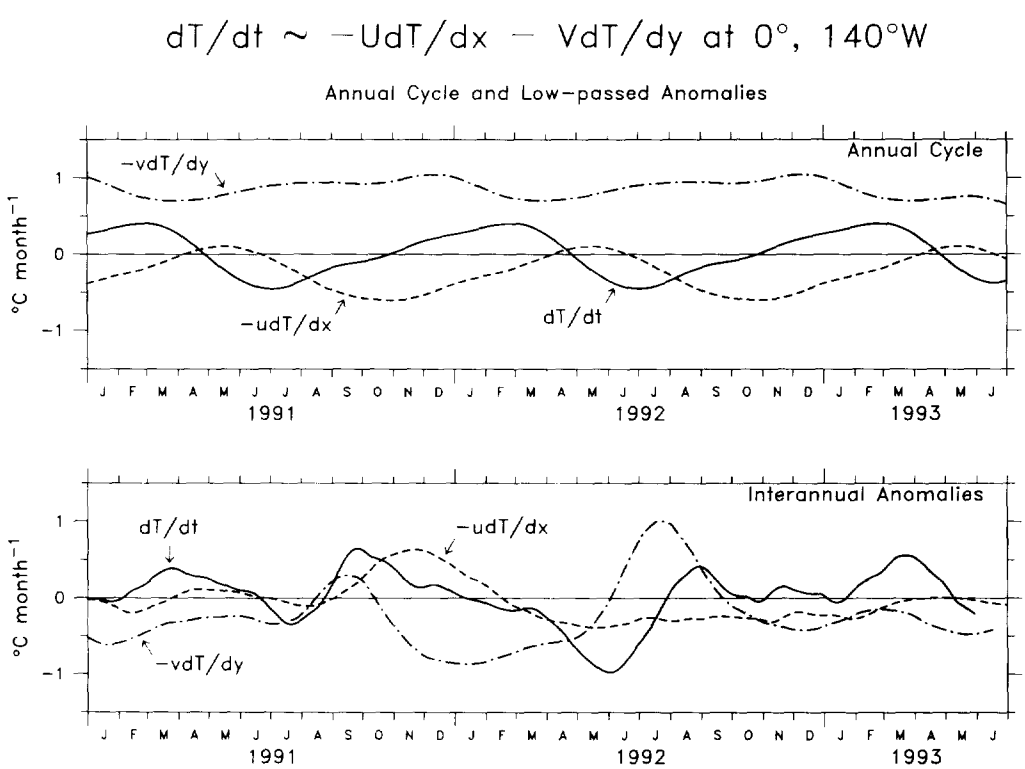

Fig. 15. Terms of the horizontal temperature advection balance at 0°, 140°W. In each panel the solid line is $\partial SST/\partial t$, the dashed line is $-u\partial SST/\partial x$, and the dash–dot line is $-v\partial SST/\partial y$. Top: the average annual cycle for 1986–1993, repeated for the 2½ years January 1991 to June 1993; bottom: interannual anomalies. All curves are drawn so that up on the plot indicates warming of the ocean.

is not clear whether this reflects a heat-flux effect on the ocean or simply coincident variability associated with the simultaneous passage of Madden–Julian signals in the atmosphere and ocean. In any case the magnitude of the LHF signals during this period was too small by a factor of four or more to have been the major factor in SST variations at this time.

With the exception of the September 1991 warming, the overall conclusion is that none of the local air–sea exchange processes could have been the primary mechanism of SST change during the El Niño; in fact during most of this period these fluxes either opposed the observed changes or were too small to be principal factors. This result is consistent with previous empirical analyses (e.g. Reed, 1986; Liu and Gautier, 1990) and modeling studies (Seagar *et al.*, 1988), which indicate ocean dynamics as the principal generating mechanism for ENSO SST anomalies, with surface heat fluxes acting as a negative feedback on their growth in the cold tongue region.

4.2 *Horizontal advection of SST*

Figure 15 shows the average annual cycle (computed for the period 1986–1993) and interannual anomalies of the terms of equation (5) during 1991 to mid-1993. The average

annual cycle shown includes the long-term mean, which is about -0.27°C month^{-1} for $-u\partial(\mathrm{SST})/\partial x$ and $+0.88$°C month^{-1} for $-v\partial(\mathrm{SST})/\partial y$ [means of the advective terms are reported with signs as in equation (5), so that positive values represent warming tendencies for the ocean]. The negative value for the zonal advective term reflects the mean westward South Equatorial Current at the surface and the negative zonal SST gradient. However, when integrated over an upper layer of 50 m thickness, the mean heat flux due to zonal advection is small (about -1 W m^{-2}; Table 1) since the mean zonal current is strongly sheared and becomes eastward below about 40 m depth. The value of heat flux computed thus depends strongly on the chosen depth of the surface "mixed" layer, so caution should be used in comparing the mean value of zonal advective heat flux reported in Table 1 with others quoted in the literature. For example, Enfield (1986) found a mean zonal advective flux of about -19 W m^{-2}, over the latitude range 5°S to 5°N, with most of this flux occurring in the SEC off the equator, where the vertical shear is much smaller. On the other hand, annual and interannual variations of central tropical Pacific zonal current tend to be vertically coherent over at least the upper 100 m (e.g. Fig. 7), so our estimates of the variability of zonal advective fluxes appear reasonably robust. Similarly, there was little shear found in the meridional velocity, either in the mean or the variability. The mean negative value for meridional advection is consistent with the net equatorward eddy heat flux associated with tropical instability waves (Hansen and Paul, 1984), and the mean meridional advective heat flux during 1986–1993 was about $+69$ W m^{-2}. Enfield (1986) found the meridional advective heat flux to be about -58 W m^{-2}, based on his 5°S to 5°N regions; as he noted, this value includes the cooling effect of advecting upwelled water from the equator into the near-equatorial region, whereas our calculation (see the introduction to Section 4) is based on meridional derivatives taken within 1.5° of the equator. The annual amplitudes of $\partial(\mathrm{SST})/\partial t$ and $u\partial(\mathrm{SST})/\partial x$ are about 0.25°C month^{-1}, and they are nearly in quadrature, with maximum actual warming of SST in February, but maximum zonal advective warming in May (Fig. 14). The annual amplitude of $v\partial(\mathrm{SST})/\partial y$ is about 0.11°C month^{-1}, and is nearly out of phase with observed SST warming. Thus the annual cycle of horizontal advection clearly does not account for the annual variation of SST.

The interannual anomalies shown in Fig. 15 were defined as the deviations from the average annual cycle, low-pass filtered with a half-power point at about 145 days. The RMS amplitude of interannual zonal advection, integrated over the upper 50 m, was about 17 W m^{-2}, and for meridional advection the corresponding value was about 38 W m^{-2} (Table 1). The interannual anomalies of $\partial(\mathrm{SST})/\partial t$ show the rapid rise of SST in September 1991, roughly four months before the usual annual warming, then strong cooling in mid-year 1992, approximately at the time that the usual annual strengthening of the cold tongue occurs in the average year (Fig. 15). Interannual zonal advective warming occurred about two months later than the observed warming, and was associated with the equatorial eastward surface current anomalies that peaked at the height of the event (Fig. 6). Interannual zonal advective cooling lasted throughout 1992 as the South Equatorial Current returned strongly at that time (Fig. 6). We note that during the 1991–1992 event, interannual variations of $u\partial(\mathrm{SST})/\partial x$ at 140°W were more strongly influenced by fluctuations of zonal current, rather than of zonal temperature gradient, i.e. $u\partial(\mathrm{SST})/\partial x \approx \overline{u}\partial(\mathrm{SST})/\partial x$, where the overbar denotes the time mean.

Interannual anomalies of meridional SST advection were large during the 1991–1992 event, and comprised a brief anomalous warming at the start of El Niño in September

1991, then strongly anomalous cooling during the height of the event, followed by warming anomalies in mid-year 1992 (Fig. 15). Except for the initial warming, $v\partial(\mathrm{SST})/\partial y$ could not have been responsible for the low-frequency variations of SST at 140°W during the El Niño, since its anomalies were opposite to what occurred in SST. Low-frequency variations of both meridional current and SST gradient were important in determining fluctuations of $v\partial(\mathrm{SST})/\partial y$ at 140°W during this period. The anomalous cooling tendency during the height of the event between November 1991 and April 1992 was due both to relatively weak meridional currents and to weak meridional SST gradients associated with a weakened cold tongue (Fig. 10). Note that the cooling anomalies cancelled the mean $v\partial(\mathrm{SST})/\partial y$, so the total term was very close to zero during this period (Fig. 15). The warming anomalies of mid-1992 were associated both with recovery of the cold tongue (hence increased meridional SST gradient) and an increase in meridional current variations related to instability waves (Fig. 11).

To examine the influence of horizontal advection on the rapid SST changes of the event, Figs 14(b) and (c) show the terms of the horizontal advective balance (5) during the onset and height of the El Niño of 1991–1992, lightly smoothed with half-power at about six days. On short timescales the zonal advective term shows the strong influence of intraseasonal Kelvin waves. The initial large warming event in September 1991 apparently was not associated with zonal advection [Fig. 14(b)]. However, during the 4-month period from late October 1991 until late February 1992 there was close agreement between the effects of zonal advection and the observed change in SST [Fig. 14(b)], indicating that this was the dominant process of the second and third warming events and intervening coolings. Figure 9 shows that these warmings occurred while the thermocline was deepening as a result of the intraseasonal Kelvin waves associated with eastward current pulses (Fig. 7). Similarly the smaller cooling events of SST between the peaks [Fig. 14(b)] are consistent with the Kelvin wave advection mechanism during this period. These results agree with the conclusions of Johnson and McPhaden (1993), who found that intraseasonal Kelvin wave advection produced SST changes of similar magnitude during the 1986–1987 El Niño. Kessler *et al.* (1995) have suggested that such Kelvin wave induced advective warmings could be part of a coupled interaction associated with the advance of westerly winds and warm SST across the basin.

The final episode of SST warming in late March 1992 occurred simultaneously with passage of the fourth Kelvin wave. However, since there was almost no zonal temperature gradient at this time the eastward current pulse associated with the wave had no apparent effect on SST at 140°W. The rapid cooling in June 1992 also seemed to have little connection with intraseasonal Kelvin wave related zonal advection, since the zonal current at the surface was weak at this time (Fig. 7). We conclude that zonal advection associated with intraseasonal Kelvin waves was the dominant mechanism affecting SST for the warming pulses observed during November 1991 to February 1992, but the initial, largest warming in September 1991, and the rapidity of the SST cooling in May to June 1992 cannot be accounted for by zonal advection.

In contrast to the zonal advective term, meridional advection was a large influence on SST at 140°W for a brief period during the initial warming in September 1991, but then remained very close to zero during the rest of the warm event of 1991–1992 [Fig. 14(c)]. The initial warming at 140°W was accentuated by the passage of a tropical instability wave (Fig. 8), which produced an abrupt rise of SST peaking just at the beginning of October 1991 (Fig. 9). Figures 8 and 4 suggest that the tropical instability waves which

occurred just as the general warming was beginning were superimposed on the zonally-coherent signal, and it is difficult to disassemble the multiple processes affecting SST at that time. We note that the SST rise occurred essentially simultaneously across a very broad range of longitudes (Fig. 8), including locations experiencing all phases of the tropical instability waves. Thus, even though at 140°W meridional advection associated with wave passage appears as a large component of the observed SST rise in late September 1991 [Fig. 14(c)], these waves cannot be taken as the cause of the general warming in the eastern and central Pacific.

4.3 *Upwelling*

Figure 16 shows the observed terms of the balance (6) at 0°, 140°W, with the constants A ($= 4.568 \times 10^6$ °C m^{-1} s^2) and T_0 ($= 29.3$°C) found by linear least squares regression between the observed SST and the ratio $\tau^x/Z23$. The time series used to compute the

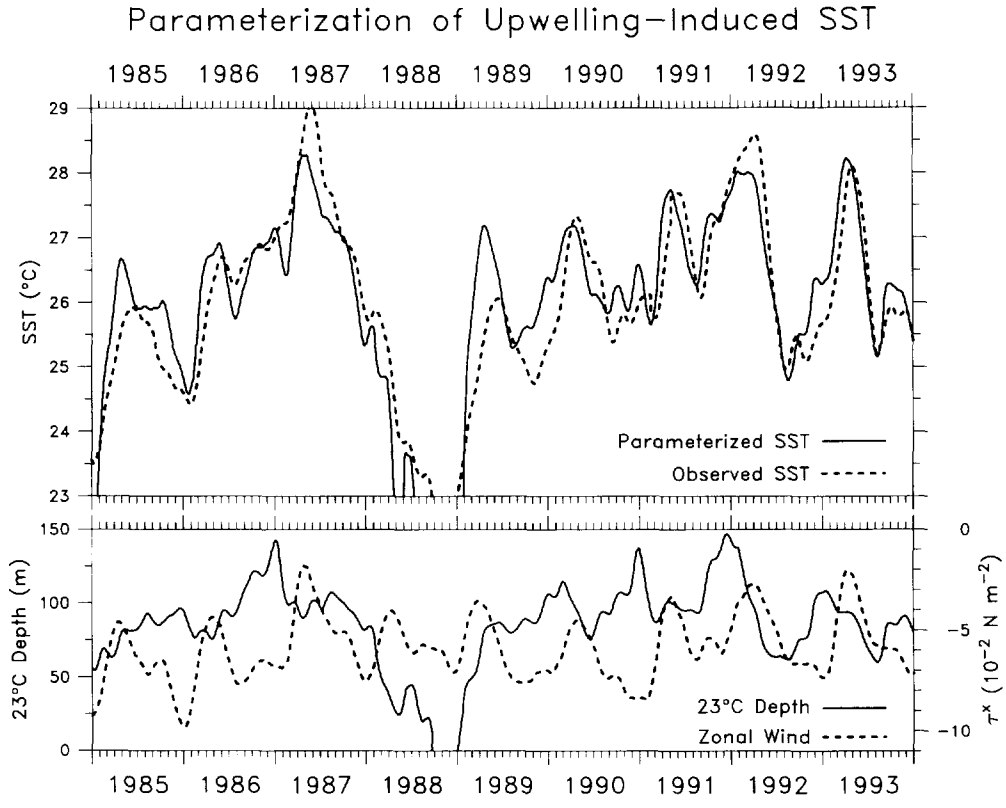

Fig. 16. The parameterization of the effect of upwelling on SST according to equation (6). Top: observed SST at 0°, 140°W (dot) and the parameterization [equation (6)] (line). Both have units of degrees centigrade. Bottom: the components used to produce (6). Zonal wind stress (10^{-2} N m^{-2}; scale at right) and 23°C depth (m; scale at left). Both have been drawn so up on the plot indicates an SST warming tendency. SST, wind stress and 23°C depth have been low-pass filtered with a half-power point of 145 days.

terms of equation (6) were low-pass filtered with a half-power point of 145 days, consistent with our assumption of a nearly steady balance (test calculations with unfiltered data gave worse agreement). Over nine years, 1985 to 1993, the correlation between observed and modeled SST was 0.80. Similar high levels of correlation between this parameterization and observed SST were found everywhere between 110°W and 170°W. Much of the discrepancy occurred during the La Niña cold event of 1988, when equation (6) would have predicted a rapid recovery to normal SST; but in fact cold SST anomalies remained in place for at least a year after the thermocline had deepened to normal levels (Fig. 16). During 1991–1993 the correlation between SST and τ^x/Z23 was 0.90. The lower panel of Fig. 16 shows the two components of the hypothesized mechanism, τ^x and Z23. These two quantities were uncorrelated with each other ($r = -0.09$), and either alone was partially correlated with SST at about $r = 0.5$. Neither factor is dominant all the time; rather, when the thermocline is deep local wind variations are paramount, but when the thermocline is shallow fluctuations of Z23 tend to be more important. A similar result also has been found in the context of model simulations (Battisti, 1988; Barnett *et al.*, 1991). Thus, we infer that the effects of upwelling on SST depend both on the strength of local Ekman divergence and on thermocline depth variations that are remotely forced by the large scale winds.

The close agreement shown in Fig. 16 suggests that reduction in upwelling efficiency was a major element of the initial rise of SST at the onset of the warm event in August–September 1991. This was associated primarily with the large increase in thermocline depth but also with the decrease in local zonal wind stress at that time (Fig. 16, bottom). Similarly, the sharp 3°C cooling of SST in May–June 1992, which we have shown cannot be accounted for by any other process, seems to have been driven by the increasing zonal winds working on the shallow thermocline at the close of the warm event (Fig. 16). Note that the thermocline at 140°W had returned to quite shallow levels by March 1992, before the SST began to cool (Fig. 9), and this apparently created conditions such that when easterlies began to re-establish themselves in late boreal spring 1992 the SST could cool quickly by upwelling. Kessler and McPhaden (1995) showed that this shoaling of the thermocline was associated with reflection at the western boundary of the upwelling Rossby wave generated by the westerly winds at the height of the event. Thus the rapid cooling at 140°W in May–June 1992 was part of the basin-scale sequence of events that terminated the El Niño, although the cooling itself depended on locally-driven upwelling.

The value found for the fitted parameter T_0 (29.3°C) gives the temperature that the model (6) would approach in the limit of zero wind or extremely deep thermocline; this value is roughly consistent with maximum observed SSTs. The value found above for the parameter A can be used to estimate a timescale for this process as follows. First, a crude estimate of the mean upwelling velocity w across the equatorial band can be made by assuming that the zonal wind is constant over the band and that w is equal to the divergence of meridional Ekman transport across the band. If $\pm y_u$ is the latitude range over which equatorial upwelling occurs, then

$$w \approx \frac{\Delta v_E}{\Delta y} \approx \frac{-2\tau^x/\beta y_u}{2y_u} = \frac{-\tau^x}{\beta y_u^2} \tag{7}$$

where v_E is the meridional Ekman transport per unit width and the Coriolis parameter f has been taken to be βy. Equation (7) suggests that the vertical velocity is roughly a few meters per day, consistent with estimates in the literature (e.g. Wyrtki, 1981; Wyrtki and

Eldin, 1982; Bryden and Brady, 1985; Halpern, 1987; Halpern and Freitag, 1987). Then, if mean dT/dz can be approximated as (SST − 23°C)/Z23, which is about 3°C/Z23 (for mean SST of 26.06°C at 0°, 140°W), we have, using parameterization (6) for the τ^x/Z23 ratio

$$w\frac{dT}{dz} \approx \frac{-\tau^x}{\beta y_u^2}\frac{3}{Z23} \approx -\frac{SST - T_0}{A}\frac{3}{\beta y_u^2} = -\alpha(SST - T_0) \quad (8)$$

where we have defined $\alpha = 3/A\beta y_u^2$ (units time^{-1}) to collect the non-temperature terms. Equation (8) suggests that α^{-1} is a time scale for upwelling-induced SST changes, given the low-frequency parameterization (6) and approximations in (7) and (8). Note that both τ^x and Z23 cancel with these assumptions, and α is a function of the fitted parameter A, the constant β, the temperature difference between the surface and thermocline, and the unknown width of the upwelling region y_u. The quadratic dependence of α on y_u means that estimation of an upwelling time scale for SST is quite sensitive to the assumed latitudinal range over which upwelling affects SST, with faster time scale for a narrower band of latitude. For y_u of 2 to 4° latitude (based on the observed width of the cold tongue in the central equatorial Pacific), the range of time scales would be approximately 20 to 80 days, consistent with our assumption of a quasi-steady balance at the 145-day smoothing used in Fig. 16.

Equations (6), (7) and (8) allow one to estimate cooling rates due to upwelling. For examples, given the mean SST at 0°, 140°W, and taking y_u to be 3° latitude, equation (8) results in a mean cooling due to upwelling of −2.2°C month^{-1}, about twice as large as the mean warming due to meridional advection (Fig. 15). A crude estimate of the heat flux due to upwelling also can be made by integrating the right side of equation (8) over an upper layer of 50 m, assuming the terms are constant in depth. This gives a mean heat flux of about −170 W m^{-2}, almost exactly balancing the residual of the other heat flux terms (171.7 W m^{-2}; Table 1). The agreement is fortuitous, given the crudeness of the estimate of vertical velocity in equation (7), the estimate of dT/dz in equation (8), and the somewhat arbitrary choice of 50 m for the upper layer in the flux integration; these produce an uncertainty in the heat flux of at least a factor of two. Similarly, the corresponding estimates of the annual and interannual RMS upwelling heat fluxes (Table 1) are difficult to determine accurately because an additional uncertainty is introduced by the choice of averaging period; inclusion of the 1988 cold event changes these magnitudes considerably (Fig. 16). Comparison to upwelling heat flux estimates discussed in the literature is not straightforward because of the distinct assumptions used in earlier studies. Wyrtki (1981) made an argument similar to equation (7) to get w, then multiplied his estimate of upwelling rate by a presumed temperature difference of 4°C between the upwelled water and SST. This suggested an upwelling heat flux of about -8.4×10^{14} W in the region 5°S to 5°N, 100°W to 170°E, or about −74 W m^{-2}. Wyrtki's estimate is similarly sensitive to the width of the region as is equation (7); our mean heat flux would be reduced to a comparable value of about −65 W m^{-2} if we had used the width $y_u = 5°$ (which, however, we believe is too wide a definition for the upwelling region). Bryden and Brady (1985) constructed a detailed mass and heat budget for the eastern equatorial Pacific using estimated geostrophic and wind-driven flows across the zonal and meridional boundaries of their region. They showed that part of the upward vertical velocity along the equator simply reflects the zonal tilt of the thermocline, and that the part of the flow which is along-isopycnal does not act to change SST. The cross-isopycnal flow was estimated to be about one-third of the total vertical transport, in a narrow upwelling region only 1.5° wide. Although

they did not cite an estimate of upwelling heat flux, the value implied by their findings is about -75 W m^{-2}.

Our estimate of mean heat flux, like Wyrtki's, does not consider the distinction between cross and along-isopycnal flow, and thus is likely to be an overestimate. We emphasize that for this reason, as well as the various uncertainties we have detailed above, the mean upwelling heat flux can only be crudely represented from equations (6), (7) and (8). It nevertheless has been useful to examine the implications of the regression fit in equation (6) to show that the results are consistent (within the large error bounds) with previous studies using different data sets and assumptions. Of course, these uncertainties in our estimate of the mean heat flux do not in any way negate the success of the parameterization (6) itself, for which the wind stress–thermocline depth ratio is an excellent predictor of SST variability.

5. SUMMARY AND CONCLUSIONS

The oceanic and surface wind anomalies of the 1991–1993 El Niño were observed better than during any previous warm event. The highly-resolved temporal sampling showed that the interannual variations were composed of a series of higher-frequency events, prominently at the 60-day Madden–Julian timescale. Westerly winds and convection oscillating at this frequency, which are usually confined west of the dateline, penetrated into the central Pacific in concert with warm SST, and generated large-amplitude downwelling equatorial Kelvin waves which carried this signal to the eastern part of the ocean. At 140°W the downwelling phase of the waves lowered the thermocline to 40 to 50 m each time, often very rapidly; for example, in late January 1992 the 20°C isotherm at 140°W dropped more than 50 m over 5 days. Such rapid oscillations might pose a problem in the interpretation of shipboard surveys. Although the oceanic Kelvin wave speed is about 2.5 m s^{-1}, and these fast signals are clearly visible in the time series, the 6 to 8 month envelope of deep thermocline anomalies moved eastward at a much slower speed of about 60 cm s^{-1}, during both the 1991–1992 and 1993 warm events (Fig. 5).

It was not until September 1991 that the observations could be interpreted unambiguously as the onset of El Niño, and we are unable to point to specific precursors that could have been used to foretell the oncoming event. However, it is likely that precursors did exist in the tropical Pacific as early as nine months before the onset, since forecast models (Zebiak and Cane, 1987) correctly predicted both the non-occurrence of El Niño in 1990 and the actual onset in September 1991 (prediction issued in January 1991; Climate Analysis Center, 1991). Unfortunately, the present state of knowledge does not yet allow these precursors to be selected out of the mixture of signals observed. It also should be noted that the same model did not forecast the return of warm conditions in 1993, so it is clear that our understanding of the conditions that produce interannual variability in the tropical Pacific remains imperfect.

Westerly wind anomalies spread eastward across the Pacific and grew in intensity during late 1991, flattening of the large-scale zonal thermocline slope along the equator by the early months of 1992. During the peak of the event the Equatorial Undercurrent at 140°W weakened (reducing the core speed from about 100 cm s^{-1} to about 20 cm s^{-1}), as has occurred in previous El Niños. On the other hand, no major changes in the North Equatorial Countercurrent were found during the event peak in late 1991 to early 1992, unlike earlier El Niños which were characterized by large increases in the NECC at this

phase. The South Equatorial Current weakened across its entire domain at 140°W (from about 7°S to 4°N), with speeds reduced to close to zero during November 1991 through February 1992. We conclude that no large eastward transport of surface water past 140°W took place, either in the SEC or the NECC, and the divergence responsible for shoaling of the west Pacific thermocline must have been accomplished principally through meridional flow in the region west of 140°W.

As the warm event ended in mid-1992, the EUC returned to near-normal speeds, while westward flow in the SEC increased strongly above climatology; the usual "springtime reversal" of the SEC did not take place. This westward surge was similar to zonal flow changes reported during earlier events. The equatorial cold tongue returned, with cold SST anomalies of about 1°C, east of about 160°W. However, the off-equatorial eastern Pacific and the western equatorial Pacific remained anomalously warm. Typical of previous events, the aftermath of the 1991–1992 El Niño left the west Pacific thermocline anomalously shallow. Strong tropical instability wave activity was observed north of the equator in the central Pacific during August 1992 to January 1993.

The relative phasing of anomalous thermocline, equatorial undercurrent and SST variations was similar to that seen during the onset of the 1986–1987 El Niño (McPhaden and Hayes, 1990), with peak downwelling anomalies in December to January, peak undercurrent weakening a month later, and warmest SST several months after that. However, the earlier event was followed by a strong cold (La Niña) period, whereas the 1991–1992 El Niño was not. Uniquely among modern El Niños, in boreal Spring 1993 a second warm event occurred, with temperatures greater than 28°C again extending east to 110°W. This event was particularly surprising since the west Pacific thermocline remained anomalously shallow leading up to the warming, contrary to a frequently-voiced theory which postulates that El Niño events follow a "buildup" of a thick warm layer in the west (Wyrtki, 1975). Kessler and McPhaden (1995) have noted that during the previous six months a series of Madden–Julian events had brought westerly wind events extending to about the dateline (Fig. 3), and they have suggested that this might be an example of the coupled instability described in Battisti (1988) producing a weak El Niño without a preceding buildup. The 1993 event was short-lived, and east Pacific SST had returned to cool conditions by July 1993.

Both the initial warming event in September 1991 and the rapid cooling in June 1992 occurred essentially simultaneously across at least 8000 km of zonal extent (Fig. 8). This remarkable feature is crucial in developing an understanding of the mechanism of onset and decay of El Niño, since it rules out purely oceanic wave processes, which are limited by the equatorial Kelvin wave speed of about 2.5 m s^{-1}. The corresponding atmospheric limit can be up to 10 times this value, and Fig. 3 shows that changes in zonal wind do commonly occur nearly simultaneously across the equatorial Pacific. The zonal coherence of the initial warming was probably due to the westerly wind anomaly which appeared essentially simultaneously between 155°E and 110°W in September 1991 (Fig. 3, bottom). This affected the ocean both by decreasing the latent heat flux to the atmosphere and by reducing the efficiency of upwelling to cool the ocean surface. The 3°C SST cooling event that ended the 1991–1992 El Niño occurred as easterlies returned to the east and central Pacific in June 1992, and the resulting strong upwelling acted on a shallow thermocline.

Although the present data set is inadequate to calculate all terms in the upper layer heat balance, indications and some conclusions can be drawn about the mechanisms of SST change at 0°, 140°W during the event. Most of the large SST variations could not have been

due to changes in air–sea heat fluxes, which were generally found to be of the wrong sign to cause the observed signals. For example, cloudiness increased and incoming short-wave flux decreased during the period when SST was rising, then returned to near-normal before the SST cooled. Changes in latent heat flux suggested an anomalous heat gain by the ocean during September 1991, and this did appear to have played a part in the onset of warming. However, the magnitude of the latent heat flux anomaly was too small by about a factor of about three to have been the primary cause of the initial warming. Moreover, during the subsequent growth of warm SST anomalies, the latent heat flux was anomalously large, opposite to what one would have expected if turbulent air–sea exchange were the main factor in generating the SST anomalies. Likewise, at the time of rapid SST cooling in June 1992 at 140°W, the latent heat flux to the atmosphere was anomalously low compared to climatology. These results suggest that air–sea heat fluxes were probably not the dominant mechanisms responsible for the observed El Niño SST anomalies at 140°W. Conversely, zonal advection of SST, particularly associated with the intraseasonal Kelvin waves, closely balanced observed SST changes during November 1991 to February 1992 near the height of the warm event, accounting for about 1°C of the SST anomalies at 140°W [Fig. 14(b)]. At lower frequencies (annual and interannual), variations of zonal SST advection were generally not well correlated with observed SST changes at 0°, 140°W, though strong westward flow in mid-1992 may have contributed about 1/3 of the observed cooling at the end of the 1991–1992 warm event. Meridional advection due to the passage of a set of tropical instability waves caused the initial SST rise at 140°W to be especially abrupt, but otherwise was apparently an anomalous cooling tendency near the equator during the 1991–1993 event.

A simple method of parameterizing the effects of upwelling on SST was developed, in which upwelling was taken to be proportional to local zonal wind stress (via Ekman divergence), but the effectiveness of upwelling to change the SST was taken to be inversely proportional to thermocline depth, which is largely remotely forced. This parameterization reproduces the observed SST changes quite well on timescales of a few months and longer (Fig. 16). These results suggest that variations in upwelling were a principal contributor to SST change during the 1991–1992 event at 140°W. In particular, the 3°C cooling in May–June 1992, which was not well accounted for by any other process, appears to have been due primarily to changes in upwelling. The parameterization emphasizes that both local wind forcing and remotely-forced thermocline variations are necessary to account for the observed SST changes in the equatorial cold tongue.

Although we have pointed to specific elements of the SST balance as being dominant at particular times, the observations presented (Figs 13–16; Table 1) indicate that all the fluxes, including the air–sea fluxes, horizontal advection, and upwelling, were important to the mean and to the annual and interannual variability of the overall balance. None of the terms were small, all had large fluctuations, and all must be accurately measured if quantification of the surface heat balance is to be achieved.

Acknowledgements—The authors would like to thank the TAO group of NOAA/PMEL for processing the raw data and preparing formatted data sets, including Paul Freitag and Tricia Pullen for the current meter mooring and ADCP data sets, Margie McCarty for the air–sea flux data, and Dai McClurg for formatted temperature data. Jerry Davison of NOAA/PMEL processed the COADS wind and SST climatologies. The TOGA XBT data set was collated and quality-controlled at the TOGA Subsurface Data Centre in Brest, France, and provided by Jean-Paul Rebert. The weekly satellite blended SST fields were produced by Dick Reynolds, Diane Stokes and Thomas Smith at the National Centers for Environmental Prediction. Support from NOAA's Equatorial Pacific

Ocean Climate Studies and Tropical Ocean/Global Atmosphere programs is gratefully acknowledged. PMEL Contribution No. 1566. U.S. JGOFS Contribution No. 137.

REFERENCES

Barnett T. P., M. Latif, E. Kirk and E. Roeckner (1991) On ENSO physics. *Journal of Climate*, **4**, 487–515.

Battisti D. S. (1988) The dynamics and thermodynamics of a warm event in a coupled atmosphere/ocean model. *Journal of Atmospheric Science*, **45**, 2889–2919.

Battisti D. S. and A. Hirst (1989) Interannual variability in a tropical ocean-atmosphere model: influence of the basic state, ocean geometry and nonlinearity. *Journal of Atmospheric Science*, **46**, 1687–1712.

Bryden H. L. and E. C. Brady (1985) Diagnostic model of the three-dimensional circulation in the upper equatorial Pacific ocean. *Journal of Physical Oceanography*, **15**, 1255–1273.

Cane M. A. (1983) Oceanographic events during El Niño. *Science*, **222**, 1189–1202.

Chang P. (1993) Seasonal cycle of sea surface temperature and mixed layer heat budget in the tropical Pacific Ocean. *Geophysical Research Letters*, **20**, 2079–2082.

Chang P. (1994) A study of the seasonal cycle of sea surface temperature in the tropical Pacific Ocean using reduced gravity models. *Journal of Geophysical Research*, **99**, 7725–7741.

Chelton D. B. and R. E. Davis (1982) Monthly mean sea level variability along the west coast of North America. *Journal of Physical Oceanography*, **12**, 757–784.

Climate Analysis Center (1991) Climate Diagnostics Bulletin, Near Real-Time Analyses, January 1991. U.S. Dept. of Commerce, National Oceanic and Atmospheric Administration, Washington, DC, U.S.A.

Enfield D. B. (1986) Zonal and seasonal variations of the near-surface heat balance of the equatorial Pacific Ocean. *Journal of Physical Oceanography*, **16**, 1038–1054.

Feng Y. I., D. E. Harrison and A. A. Lacis (1984) On the variability of the net longwave radiation at the ocean surface. *Reviews of Geophysics and Space Physics*, **22**, 177–193.

Firing E., R. Lukas, J. Sadler and K. Wyrtki (1983) Equatorial Undercurrent disappears during the 1982–1983 El Niño. *Science*, **222**, 1121–1123.

Freitag H. P., Y. Feng, L. J. Mangum, M. J. McPhaden, J. Neander and L. D. Stratton (1994) Calibration Procedures and Instrumental Accuracy Estimates of TAO Temperature, Relative Humidity and Radiation Measurements. NOAA Tech. Mem. ERL/PMEL 1589, Seattle, WA, U.S.A.

Halpern D. (1987) Observations of annual and El Niño flow variations at 0°, 110°W and 0°, 95°W during 1980–1985. *Journal of Geophysical Research*, **92**, 8197–8212.

Halpern D. and H. P. Freitag (1987) Vertical motion in the upper ocean of the equatorial eastern Pacific. *Oceanologica Acta*, **6**(SP), 19–26.

Halpern D., R. A. Knox and D. S. Luther (1988) Observations of 20-day period meridional current oscillations in the upper ocean along the Pacific equator. *Journal of Physical Oceanography*, **18**, 1514–1534.

Hansen D. V. and C. A. Paul (1984) Genesis and effects of long waves in the equatorial Pacific. *Journal of Geophysical Research*, **89**, 10,431–10,440.

Hayes S. P., L. J. Mangum, J. Picaut, A. Sumi and K. Takeuchi (1991a) TOGA/TAO: A moored array for real-time measurements in the tropical Pacific Ocean. *Bulletin of the American Meteorological Society*, **72**, 339–347.

Hayes S. P., P. Chang and M. J. McPhaden (1991b) Variability of the sea surface temperature in the eastern equatorial Pacific during 1986–1988. *Journal of Geophysical Research*, **96**, 10,553–10,566.

Johnson E. S. and M. J. McPhaden (1993) On the structure of equatorial Kelvin waves in the Pacific Ocean. *Journal of Physical Oceanography*, **13**, 608–625.

Kerr R. A. (1990) Who will win the El Niño sweepstakes this time? *Science*, **248**, 445.

Kerr R. A. (1991) El Niño winners and losers declared. *Science*, **251**, 1182.

Kessler W. S. (1990) Observations of long Rossby waves in the northern tropical Pacific. *Journal of Geophysical Research*, **85**, 5183–5217.

Kessler W. S. and B. A. Taft (1987) Dynamic heights and zonal geostrophic transports in the central tropical Pacific during 1979–84. *Journal of Physical Oceanography*, **17**, 97–122.

Kessler W. S., M. J. McPhaden and K. M. Weickmannn (in press) Forcing of intraseasonal Kelvin waves in the equatorial Pacific. *Journal of Geophysical Research*.

Kessler W. S. and M. J. McPhaden (in press) Equatorial waves and the dynamics of the 1991–93 El Niño. *Journal of Climate*.

Legeckis R. (1977) Long waves in the eastern equatorial Pacific Ocean: A view from a geostationary satellite. *Science*, **197**, 1179–1181.

Levitus S. (1982) *Climatological Atlas of the World Ocean*. NOAA Prof. Paper 13, U.S. Gov't Printing Office, Washington, DC, U.S.A., 173 pp.

Liu W. T. and C. Gautier (1990) Thermal forcing on the tropical Pacific from satellite data. *Journal of Geophysical Research*, **95**, 13,209–13,217.

Liu W. T., K. B. Katsaros and J. A. Businger (1979) Bulk parameterization of air–sea exchanges of heat and water vapor including molecular constraints at the interface. *Journal of Atmospheric Science*, **36**, 1722–1181.

Madden R. A. and P. R. Julian (1971) Detection of a 40–50 day oscillation in the zonal wind in the tropical Pacific. *Journal of Atmospheric Science*, **28**, 702–708.

Madden R. A. and P. R. Julian (1972) Description of global-scale circulation cells in the tropics with a 40–50 day period. *Journal of Atmospheric Science*, **29**, 1109–1123.

McCreary J. P. (1983) A model of tropical ocean–atmosphere interaction. *Monthly Weather Review*, **111**, 370–387.

McPhaden M. J. (1993) TOGA/TAO and the 1991–93 El Niño-Southern Oscillation event. *Oceanography*, **6**, 36–44.

McPhaden M. J. (submitted) Monthly period oscillations in the Pacific North Equatorial Countercurrent. *Journal of Geophysical Research*.

McPhaden M. J. and S. P. Hayes (1990) Variability in the eastern equatorial Pacific Ocean during 1986–1988. *Jouurnal of Geophysical Research*, **95**, 13,195–13,208.

McPhaden M. J. and J. Picaut (1990) El Niño-Southern Oscillation displacements of the western equatorial Pacific warm pool. Science, **250**, 1385–1388.

McPhaden M. J. and M. J. McCarty (1992) Mean Seasonal Cycles and Interannual Variations at 0°, 110°W and 0°, 140°W During 1980–1991. NOAA Data Report ERL-PMEL-95, U.S. Dept Commerce, Washington DC, 118 pp.

McPhaden M. J., S. P. Hayes, L. J. Mangum and J. M. Toole (1990) Variability in the western equatorial Pacific Ocean during the 1986–87 El Niño/Southern Oscillation event. *Journal of Physical Oceanography*, **20**, 190–208.

Meyers G. and J.-R. Donguy (1984) The North Equatorial Countercurrent and heat storage in the western Pacific during 1982–83. *Nature*, **312**, 258–260.

Murray J. W., R. T. Barber, M. R. Roman, M. P. Bacon and R. A. Feely (1994) Physical and biological controls on carbon cycling in the equatorial Pacific. *Science*, **266**, 58–65.

Oberhuber J. M. (1988) An atlas based on the COADS data set: The budgets of heat, buoyancy, and turbulent kinetic energy at the surface of the global ocean. Report No. 15, Max Planck Institute for Meteorology, Hamburg, Germany, 20 pp.

Picaut J. and R. Tournier (1991) Monitoring the 1979–1985 equatorial Pacific current transports with expendable bathythermograph data. *Journal of Geophysical Research*, **96**, 3263–3277.

Picaut J. and T. Delcroix (in press) Equatorial wave sequence associated with warm pool displacements during the 1986–1989 El Niño–La Niña. *Journal of Geophysical Research*.

Pullen P. E., R. L. Bernstein and D. Halpern (1987) Equatorial long-wave characteristics determined from satellite sea surface temperature and *in situ* data. *Journal of Geophysical Research*, **92**, 742–748.

Reed R. K. (1983) Heat fluxes over the eastern tropical Pacific and aspects of the 1972 El Niño. *Journal of Geophysical Research*, **88**, 9627–9638.

Reed R. K. (1986) Effects of surface heat flux during the 1972 and 1982 El Niño episodes. *Nature*, **322**, 449–450.

Reynolds R. W. (1988) A real-time global sea surface temperature analysis. *Journal of Climatology*, **1**, 75–86.

Reynolds R. W. and T. M. Smith (1994) Improved global sea surface temperature analyses using optimum interpolation. *Journal of Climate*, **7**, 929–948.

Rui H. and B. Wang (1990) Development characteristics and dynamic structure of tropical intraseasonal convection anomalies. *Journal of Atmospheric Science*, **47**, 357–379.

Seager R., S. E. Zebiak and M. A. Cane (1988) A model of the tropical Pacific sea surface temperature climatology. *Journal of Geophysical Research*, **93**, 1265–1280.

Suarez M. J. and P. S. Schopf (1989) A delayed action oscillator for ENSO. *Journal of Atmospheric Science*, **45**, 549–566.

Taft B. A. and W. S. Kessler (1991) Variations of zonal currents in the central tropical Pacific during 1970 to 1987: Sea level and dynamic height measurements. *Journal of Geophysical Research*, **96**, 12,599–12,618.

Wakata Y. and W. S. Sarachik (1991) Unstable coupled ocean-atmosphere basin modes in the presence of a spatially-varying basic state. *Journal of Atmospheric Science*, **48**, 2060–2077.

Waliser D. E., N. E. Graham and C. Gautier (1993) Comparison of highly reflective cloud and outgoing longwave radiation datasets for use in estimating tropical deep convection. *Journal of Climatology*, **6**, 331–353.

Weickmann K. M. and S. J. S. Khalsa (1990) The shift of convection from the Indian Ocean to the western Pacific Ocean during a 30–60 day oscillation. *Monthly Weather Review*, **118**, 964–978.

Weickmann K. M., G. R. Lussky and J. E. Kutzbach (1985) Intraseasonal (30–60 day) fluctuations of outgoing long-wave radiation and 250 mb streamfunction during northern winter. *Monthly Weather Review*, **113**, 941–961.

White W., G. Meyers, J.-R. Donguy and S. Pazan (1985) Short-term climate variability in the thermal structure of the Pacific Ocean during 1979–82. *Journal of Physical Oceanography*, **17**, 917–935.

Woodruff S. D., R. J. Slutz, R. L. Jenne and P. M. Steurer (1987) A Comprehensive Ocean–Atmosphere Data Set. *Bulletin of the American Meteorological Society*, **68**, 1239–1250.

Wyrtki K. (1974) Sea level and the seasonal fluctuations of the equatorial currents in the western Pacific Ocean. *Journal of Physical Oceanography*, **4**, 91–103.

Wyrtki K. (1975) El Niño: the dynamic response of the equatorial Pacific to atmospheric forcing. *Journal of Physical Oceanography*, **5**, 572–584.

Wyrtki K. (1979) The response of sea surface topography to the 1976 El Niño. *Journal of Physical Oceanography*, **9**, 1223–1231.

Wyrtki K. (1981) An estimate of equatorial upwelling in the Pacific. *Journal of Physical Oceanography*, **11**, 1205–1214.

Wyrtki K. (1984) The slope of sea level along the equator during the 1982/1983 El Niño. *Journal of Geophysical Research*, **89**, 10,419–10,424.

Wyrtki K. and G. Eldin (1982) Equatorial upwelling events in the central Pacific. *Journal of Physical Oceanography*, **12**, 984–988.

Zebiak S. E. and M. A. Cane (1987) A model El Niño–Southern Oscillation. *Monthly Weather Review*, **115**, 2262–2278.

Zhang G. J. and M. J. McPhaden (1995) On the relationship between sea surface temperature and latent heat flux in the equatorial Pacific. *Journal of Climate*, **8**, 589–605.